EVANISE SILVA PENIDO

MECHANISMS OF CADMIUM AND LEAD RETENTION BY NOVEL PHOSPHORUS/MAGNESIUM-ENGINEERED BIOCHAR

LAVRAS – MG

2019

EVANISE SILVA PENIDO

MECHANISMS OF CADMIUM AND LEAD RETENTION BY NOVEL PHOSPHORUS/MAGNESIUM-ENGINEERED BIOCHAR

Tese apresentada à Universidade Federal de Lavras, como parte das exigências do Programa de Pós-Graduação em Agroquímica, para a obtenção do título de Doutora.

Profa. Dra. Maria Lucia Bianchi
Orientadora

Prof. Dr. Leônidas Carrijo Azevedo Melo
Coorientador

LAVRAS – MG
2019

Ficha catalográfica elaborada pelo Sistema de Geração de Ficha Catalográfica da Biblioteca Universitária da UFLA, com dados informados pelo(a) próprio(a) autor(a).

Penido, Silva Evanise.
Mechanisms of cadmium and lead retention by novel phosphorus/magnesium-engineered biochar / Evanise Silva Penido. - 2019.
72 p.

Orientadora: Maria Lucia Bianchi.
Coorientador(a): Leônidas Carrijo Azevedo Melo
Tese (doutorado) - Universidade Federal de Lavras, 2019.
Bibliografia.

1. Poultry litter. 2. Co-pyrolysis. 3. Adsorption mechanisms. I. Bianchi, Maria Lucia. II. Melo, Leônidas Carrijo Azevedo. III. Título.

EVANISE SILVA PENIDO

MECHANISMS OF CADMIUM AND LEAD RETENTION BY NOVEL PHOSPHORUS/MAGNESIUM-ENGINEERED BIOCHAR

MECANISMOS DE RETENÇÃO DE CÁDMIO E CHUMBO POR BIOCARVÕES FUNCIONALIZADOS COM FÓSFORO E MAGNÉSIO

Tese apresentada à Universidade Federal de Lavras, como parte das exigências do Programa de Pós-Graduação em Agroquímica, para a obtenção do título de Doutora.

APROVADA em 26 de Agosto de 2019.

Prof. Dr. Fabiano Magalhães	UFLA
Prof. Dr. Marcelo Braga Bueno Guerra	UFLA
Prof. Dr. Guilherme Max Dias Ferreira	UFLA
Prof. Dr. Fábio Luiz Pissetti	UNIFAL

Profa. Dra. Maria Lucia Bianchi
Orientadora

Prof. Dr. Leônidas Carrijo Azevedo Melo
Coorientador

LAVRAS – MG
2019

ACKNOWLEGMENTS

Firstly, I would like to thank God for all His protection and blessings.

Nobody has been more important to me in the pursuit of this project than the members of my family and my closest friends, who always provide unending inspiration. I am also grateful to my partner, Alan Filipe, and his parents, who have always supported me. This thesis stands as a testament to your unconditional love and encouragement.

I have great pleasure in acknowledging my advisors Prof. Dr. Maria Lucia Bianchi, Prof. Dr. Leônidas Carrijo Azevedo Melo and Prof. Dr. Luiz Roberto Guimarães Guilherme for the continuous support of my Ph.D study, for their patience, motivation, and immense knowledge. Your advice on both research as well as on my career have been invaluable. I could not have imagined having a better support.

Besides my advisors, I would like to thank my thesis committee: Prof. Dr. Fabiano Magalhães, Prof. Dr. Marcelo Braga Bueno Guerra, Prof. Dr. Guilherme Max Dias Ferreira and Prof. Dr. Fábio Luiz Pissetti, for their insightful comments and encouragement. I also gratefully thank Dr. Eliane Cristina de Resende and Dr. Lidiany Mendonça Zacaroni Lima.

I thank my fellow doctoral students and labmates for their feedback, cooperation and friendship. In addition, I would like to express my gratitude to the staff of the Chemistry Department and the Soil Science Department, as well as to the Federal University of Lavras (UFLA).

This work would not have been possible without the financial support and scholarship provided by Fundação de Amparo a Pesquisa do Estado de Minas Gerais – FAPEMIG and Conselho Nacional de Desenvolvimento Científico e Tecnológico – CNPq. This study was financed in part by the Coordenação de Aperfeiçoamento de Pessoal de Nível Superior – Brasil (CAPES) – Finance Code 001. I also thank Laboratório Nacional de Luz Síncrotron – LNLS, Centro de Tecnologias Estratégicas do Nordeste – CETENE, and Instituto de Física "Gleb Wataghin" for analysis support.

Last but not least, I dedicate this thesis and degree to my sweet high school teacher, Manu (Emmanuela Vitorino). She was the first teacher to ever believe in my potential. Words cannot express how much you have influenced me.

This accomplishment would not have been possible without you all.

THANK YOU!

RESUMO

Neste estudo, biocarvões funcionalizados com fósforo/magnésio foram preparados a partir da co-pirólise da cama de frango e fontes de fosfato e óxido de magnésio (MgO) e testados quanto às capacidades de retenção de cádmio (Cd^{2+}) e chumbo (Pb^{2+}), elucidando os mecanismos de adsorção. No primeiro artigo, que foi publicado na Science of the Environment Total Journal (Elsevier), experimentos de adsorção em batelada foram conduzidos para avaliar a capacidade de adsorção de Cd^{2+} pelos biocarvões, utilizando uma ampla gama de técnicas de caracterização para elucidação dos mecanismos de retenção. Os resultados mostraram que, em geral, a remoção de Cd^{2+} não mudou drasticamente com a variação inicial do pH e foi relativamente rápida (até 3 h). As superfícies dos biocarvões contêm uma rica variedade de grupos funcionais contendo oxigênio e fósforo. Como as áreas de superfície específicas dos biocarvões são consideradas baixas (25,19 m^2 g^{-1}), os grupos de superfície contribuíram mais para a retenção de Cd^{2+}, e complexação e precipitação foram os mecanismos de adsorção predominantes. Portanto, os biocarvões funcionalizados com P/Mg são considerados adsorventes eficazes e de baixo custo para remoção de Cd^{2+} do meio aquoso. No segundo estudo, determinou-se a eficiência de remoção de Pb^{2+} pelos biocarvões por meio de ensaios em batelada e os mecanismos de retenção foram elucidados utilizando métodos avançados de caracterização. As adsorções de Pb^{2+} pelos biocarvões funcionalizados (600 mg g^{-1}) foram quase 10 vezes mais eficazes do que o biocarvão não tratado (60 mg g^{-1}). Os grupos funcionais na superfície dos biocarvões são modificados durante a adsorção, especialmente grupos contendo fósforo e oxigênio. Os teores de P e Mg aumentaram após a modificação, mostrando alta correlação entre o Pb adsorvido e P e O, que interagiram com Pb através da quimissorção (especialmente precipitação e complexação). O tratamento com compostos de fosfato e MgO causou a formação de apatitas de chumbo insolúveis na superfície dos biocavões modificados, bem como outros componentes cristalinos inorgânicos de Pb, incluindo ($Pb_3(CO_3)_2(OH)_2$) e $PbCO_3$, como observado nos padrões de difração de Raio-X (DRX), e confirmado por espectroscopia de absorção de Raio-X (XAS). Assim, os biocarvões funcionalizados com P/Mg e produzidos a partir de cama de frango são considerados adsorventes eficazes e ecologicamente corretos para ambientes aquosos contaminados com Pb, como águas residuais. Como os mecanismos de retenção foram profundamente investigados, o presente estudo fornece base para uma aplicação prática bem-sucedida dos materiais na remediação ambiental em relação à contaminação por Pb e Cd.

Palavras-chave: Cama de frango. Co-pirólise. Mecanismos de adsorção. Contaminação.

ABSTRACT

In this study, novel phosphorus/magnesium-engineered biochars were prepared from co-pyrolysis of poultry litter and phosphate sources and magnesium oxide (MgO) and tested for their cadmium (Cd^{2+}) and lead (Pb^{2+}) retention capacities, unraveling the adsorption mechanisms. In the first article, which was published at Science of the Total Environment Journal (Elsevier), batch experiments were conducted to evaluate the adsorption ability of Cd^{2+} by biochars and a wide range of characterization techniques were used. Results showed that, in general, Cd^{2+} removal did not drastically change with initial pH variation and was relatively fast (up to 3 h). The surfaces of the biochars contain a rich variety of oxygen-containing functional groups as well as phosphate groups. Since the specific surface areas of the biochars are considered low (up to 25.19 $m^2\ g^{-1}$), surface groups contributed more to Cd^{2+} retention. Complexation and precipitation were the predominant adsorption mechanisms. Thus, P/Mg-engineered biochars are considered effective and eco-friendly adsorbents for Cd^{2+} removal from aqueous medium. In the second study, it was determined the efficiency of Pb^{2+} removal by phosphorus/magnesium-engineered biochars through batch assays and the retention mechanisms were elucidated, using advanced characterization methods. Adsorptions of Pb^{2+} by the P/Mg-engineered biochars (up to 600 mg g^{-1}) were nearly 10 times more effective than the non-treated biochar (60 mg g^{-1}). The functional groups on the surface of the biochars are modified during adsorption, especially phosphorus and oxygen-containing groups. The contents of P and Mg increased after modification, showing high correlation between adsorbed Pb and P and O, which interacted with Pb through chemisorption (especially precipitation and complexation). Treatment with phosphate compounds and MgO, which increased the pH of the biochars, caused the formation of insoluble lead apatites on the surface of the P/Mg-engineered biochars, as well as other Pb inorganic crystalline components, including $Pb_3(CO_3)_2(OH)_2$ and $PbCO_3$, as observed in the X-ray diffraction (XRD) patterns, and confirmed by X-ray absorption spectroscopy (XAS). Thus, P/Mg-engineered biochars produced from poultry litter are considered effective and eco-friendly adsorbents for Pb-contaminated aqueous environments, such as wastewater. Since the retention mechanism was deeply investigated, this study provides a basis for a successful practical application of the biochars in environmental remediation regarding Pb and Cd contamination.

Keywords: Poultry litter. Co-pyrolysis. Adsorption mechanisms. Contamination.

SUMMARY

PART ONE

1 INTRODUCTION

Potentially toxic metals, such as cadmium (Cd) and lead (Pb), are stable and persistent environmental pollutants that can enter the human body through the food chain, causing irreversible physiological damages (KABATA-PENDIAS, 2011). Due to their extreme toxicity, especially in the aquatic environment, it is important to find appropriate treatment. Adsorption has attracted attention as an effective purification and separation technique for treating wastewater (LEE; PARK; CHUNG, 2019). In this way, biochars produced from residues are often considered suitable low-cost adsorbents (WANG; WANG, 2019).

Biochar is produced by the thermochemical decomposition of biomass in the absence of oxygen, a process known as pyrolysis (GUIZANI et al., 2016). To further improve its environmental contaminant retention capacity, the feedstock can be treated with other compounds, such as phosphorus and magnesium, which leads to structural modifications of the final composite, improving its adsorption capacity (PREMARATHNA et al., 2019).

Recent studies have pointed out the importance of understanding the different adsorption mechanisms (WANG; WANG, 2019; WANG et al. 2019). Despite many studies have been performed on biochar and Cd^{2+} and Pb^{2+} adsorption from aqueous solution (CHEN et al., 2019; JAZINI;SOLEIMANI; MIRGHAFFARI, 2018), studies exploring in details the retention mechanisms by using a wide range of characterization techniques using novel engineered biochars are still incipient.

Therefore, this thesis study aimed to investigate Cd^{2+} and Pb^{2+} retention capacities of phosphorus/magnesium-engineered biochars produced from poultry litter through batch adsorption assays, exploring their physicochemical properties in order to unravel and quantify the adsorption mechanisms. Part two of this thesis presents one article published at Science of the Total Environment Journal titled “Cadmium binding mechanisms and adsorption capacity by novel phosphorus/magnesium-engineered biochars” (PENIDO et al., 2019) and one manuscript focusing on Pb retention, which is titled “Spectroscopic investigation of Pb^{2+} retention on phosphorus/magnesium-engineered biochars”.

2 LITERATURE REVIEW

This section includes a literature review, providing foundation of knowledge on the research topic.

2.1 Potentially toxic elements

The environmental pollution of soils and waters due to the release of potentially toxic elements, such as cadmium (Cd), lead (Pb), among others, has caused worldwide concern due to the high toxicity and bioaccumulation of these metals (BAIRD and CANN, 2011). Potentially toxic elements can be derived from the soil source material (lithogenic source) and from various anthropogenic sources. The main sources of release of these elements are the wastewater from chemical industries and mining activities.

For example, Pb is considered to be one of the most toxic metals, and its inorganic forms are absorbed by ingestion of food and water and by inhalation. Lead poisoning also causes inhibition of hemoglobin synthesis, dysfunctions in the kidneys, joints and reproductive systems, cardiovascular system and acute and chronic damage to the central nervous system and the peripheral nervous system. It is estimated that exposure to Pb causes about 674,000 deaths per year and 9.8% of idiopathic intellectual disability. Children are particularly vulnerable to Pb toxicity, which can adversely affect their brain and nervous system (NAGAJYOTI; LEE & SREEKANTH, 2010).

Cadmium is toxic at extremely low levels. In humans, long-term exposure may result in renal dysfunction or in lung diseases, bone defects, increased blood pressure and myocardial dysfunction (YOUNG, 2005).

Thus, in addition to health damage, high levels of toxic metals also affect the ecosystem, bringing deleterious effects, requiring care and decontamination actions.

2.2 Poultry litter production

The broiler production has grown significantly throughout the world and it is the most prominent segment in the Brazilian agribusiness. However, the waste generated in the poultry sector becomes a concern due to its accumulation and difficulty of final disposal, demanding increasingly sustainable reuse alternatives. One of the residues generated in the process is

poultry litter, which is a mixture of poultry excreta, spilled feed, feathers, and material used as bedding in poultry operations (SHAKYA & AGARWAL, 2017).

Brazil is the second largest producer of broilers in the world and the largest exporter, considering the 2018 ranking (EMPRESA BRASILEIRA DE PESQUISA AGROPECUÁRIA, 2019). It is estimated that the annual volume of waste generated in poultry production is 8 to 10 million tons per year (DALÓLIO et al., 2017). This calculation is based on the number of chickens slaughtered annually multiplied by the volume of waste generated in the process (DALÓLIO et al., 2017).

A large part of the residue produced by the poultry industry is applied in agriculture as a source of nutrients, due to high levels of nitrogen, phosphorus, and potassium (BOLAN et al., 2010). However, environmental concerns associated with such application include the presence of pathogens such as *Escherichia coli* and *Salmonella* that might be present in the material (HAHN et al., 2012). Poultry litter had already been widely used to feed cattle. However, this practice has been banned in several countries to ensure the safety of the health of animals and the population as a whole. Specifically in Brazil, according to the Normative Instruction No. 8 of March 25, 2004 (MINISTÉRIO DA AGRICULTURA, PECUÁRIA E ABASTECIMENTO, 2004), the production, commercialization, and use of products intended for ruminant feeding containing proteins and fats of animal origin is prohibited.

Thus, considering the expansion of poultry farming in Brazil and the problems related to poultry litter reuse and/or disposal, there will be greater demands for more sustainable poultry production systems and better utilization of the residues generated in animal production (EMPRAPA, 2019). Since it is necessary to seek alternatives that result in less impact to the environment, generating co-products with higher added value, the thermochemical conversion of poultry litter into biochar is considered an economically sustainable alternative for its reuse.

2.3 Pyrolysis

Pyrolysis is the thermochemical decomposition of biomass in the absence of oxygen, involving irreversible changes in the chemical composition of the material. It consists of a technique that provides a wide range of products including liquids (bio-oil), solids (biochar) and gas (biogas) (TRIPATHI et al., 2016). These co-products are obtained in different proportions depending on parameters such as heating rate, final temperature, residence time, pyrolysis atmosphere, and reactor/furnace type (LEE et al. 2017).

In the literature, it can be found studies that deal with the three types of products generated during pyrolysis. For example, Clark et al. (2017) analyzed the rate of gas emission during pyrolysis of poultry litter, analyzing the implications for the greenhouse effect and assessments of the life cycle of nitrogen. Based on the mass balance of the system, the authors found that 23-25% of the total mass of the feedstock was emitted as gas, while 52-55% and 23% were converted into bio-oil and biochar, respectively. Carbon dioxide (CO_2) and NH_3 were the predominant bulk gas species, representing 58 and 65% of the total mass emitted, respectively. Brassard, Godbout & Raghavan (2017) obtained a 50% yield of bio-oil during the pyrolysis of poultry.

One of the main advantages of the pyrolysis technique is that it can be optimized according to the desired results, since changes in the pyrolysis conditions can shape the texture and characteristics of the final products, especially the yield. Among the parameters of the process, temperature is the main factor that controls the yield of the biochar and its quality. Temperatures between 450 and 600 °C, depending on the nature and type of biomass, are the most suitable for the production of biochar. Song and Guo (2012) produced poultry litter biochars at different pyrolysis temperatures and observed that the yield, total N content, organic carbon content, and cation exchange capacity of the biochars decreased with an increase in pyrolysis temperature (from 300 to 600 ° C). On the other hand, carbon stability, surface area (BET), pH, and electrical conductivity increased with increasing pyrolysis temperature. The highest biochar yield, N contents, and cation exchange capacity values were found for the temperature of 300 °C, while the product generated at 500 °C showed the largest recalcitrant carbon mass. The authors recommend that a low pyrolysis temperature, between 300 and 500 °C, is suitable for the production of biochar from poultry litter.

2.4 Biochar: applications

Biochar is any source of biomass that underwent heat treatment in the absence or under conditions of low oxygen content (LEHMANN et al., 2012), being a solid product rich in carbon (65-90%) that contains numerous pores and functional groups containing oxygen and aromatic compounds. Biochar has the potential to improve soil productivity (NAEEM et al., 2017), to remediate contaminated environments, and to mitigate climate change (QAMBRANI et al., 2017). Such benefits, coupled with the fact that biochar can be produced by several low-cost sources of biomass, stimulate research in the area.

Initially applied to soil, the use of biochar for the removal of organic contaminants and toxic elements from aqueous media is a relatively new and promising technology for wastewater treatment (QAMBRANI et al., 2017). Cao et al. (2009) and Lu et al. (2012) found that biochars produced from residues (dairy manure and sludge) were more effective than commercial activated carbon in lead adsorption. Inyang et al. (2012) found that Pb adsorption capacity of two biochars (digested dairy waste biochar and digested sugar beet biochar) was comparable to that of commercial activated carbon, thus demonstrating that biochar produced from waste can be used as alternative adsorbents to treat wastewater.

2.5 Surface modification of biochar

The type and concentration of functional groups on the surface of the biochar play important roles in the adsorption capacity and in the explanation of adsorbent removal mechanisms (PREMARATHNA et al., 2019).

The application of different methods of surface modification in the production of biochars results in high efficiency materials with comparable adsorption capacities or even overcoming some commercial activated carbon (INYANG et al., 2016).

The surface chemistry of carbon materials is governed by basal or edge carbon atoms. The physical structure of the carbons has aromatic rings, such as sp^2 hybridization carbons, bonded by van der Waals interactions (BANDOSZ, 2006). The surface of the biochar also contains chemically active groups (OH, COOH and ketones, etc.), which, together with the aromatic structure containing π electron density on the basal plane, give the potential material to adsorb toxic metals and other substances toxic.

Biochars can be produced with infinite possibilities of structures, having good ability to react with other heteroatoms, such as phosphorus (P), during pyrolysis. Such heteroatoms may exert a great influence on the physical-chemical properties of the materials (BANDOSZ, 2006).

When mixed with biomass, compounds containing P act on the cleavages of the chemical bonds during the pyrolysis process, forming phosphate and polyphosphate bonds that are distributed along the matrix, leading to a porous structure and the creation of surface groups, in addition to the oxygen groups existing on the surface (BANDOSZ, 2006).

Pretreatment of biomass with P-containing materials increases the fertility of the biochar, while strengthening its ability to absorb toxic metals (ZHAO et al, 2016). Zhao et al. (2016) have shown that multiple beneficial functions of biochar can be achieved

simultaneously through co-pyrolysis with phosphate fertilizers. For example, the mono-ammonium-phosphate (MAP) fertilizer is formed from the reaction of ammonia with phosphoric acid and has between 10% and 12% N and 50% to 52% P_2O_5. MAP is an effective universal fertilizer and especially suitable for crops with a high requirement of P (for example maize). Triple superphosphate (TSP) has a high concentration of phosphorus, from 45 to 46%, and is one of the most used fertilizers in the world, especially in no-tillage areas of crops such as soybeans.

Lustosa Filho et al. (2017) found that phosphate sources (MAP, TSP and H_3PO_4) combined with MgO during poultry litter co-pyrolysis generate slow-release phosphate fertilizers with high potential to increase P uptake by the plant and crop growth such as corn, for example. The authors found phosphate compounds in the structure of the biochars, indicating surface functionalization with phosphate compounds. X-ray diffraction showed the main minerals present in the samples with the formation of compounds of low solubility $Ca_2P_2O_7$ and $Mg_2P_20_7$. Such groups can act actively in metal metal retention processes, thus evidencing the importance of understanding the mechanisms of interaction.

Figure 1 illustrates some species of oxygen (a) and phosphorus (b) present on the surface of biochars.

Figure 1. Illustration of biochar structures showing some species of oxygen (a) and phosphorus (b).

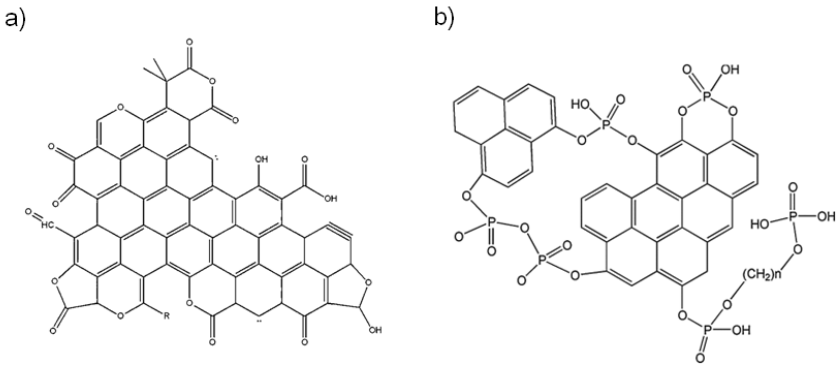

Source: adapted from Bandosz (2006).

2.6 Mechanisms of metal retention and instrumental characterization techniques

Among the various effluent treatment technologies, adsorption has received significant attention in recent years due to its rapid rate of toxic metal removal, low cost, cost-effectiveness, ease of operation and high efficiency (LEE; PARK; CHUNG, 2019).

Several mechanisms of action for the removal of pollutants using biochars have been reported in the literature, including precipitation, complexation, ion exchange and physical adsorption (Figure 2).

Figure 2. Illustration of mechanisms of metal ions removal by biochar.

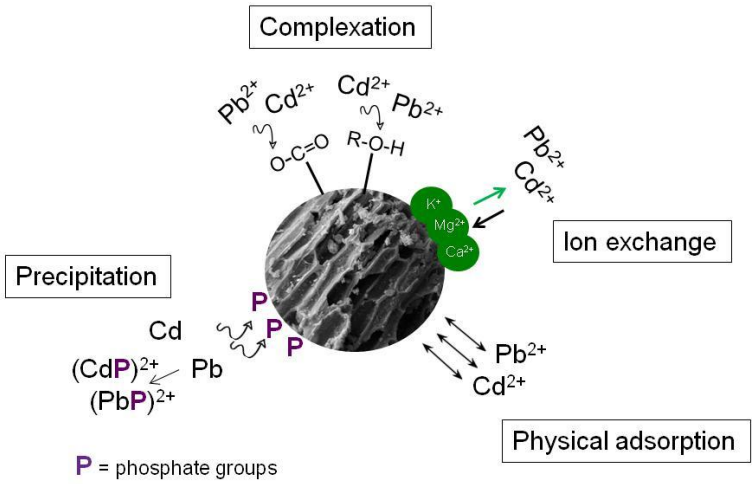

Source: from author (2019).

In general, the physical or superficial adsorption describes the removal of toxic metals by the diffusion movement of metallic ions into sorbent pores, without the formation of chemical bonds. Ionic exchange occurs through a selective substitution of positively charged ions from the biochar surfaces with metal species in solution and is related to the cation exchange capacity of the carbonaceous material. Complexation, which may be of the inner or outer sphere, involves the formation of multi-atom structures, representing complexes with specific metal-binding interactions. This mechanism is of great importance for metals, especially transition metals with partially filled d orbitals with high affinity for ligands (SHRIVER and ATKINS, 2008). Precipitation is the formation of solids, which may occur both in solution and on the surface, during adsorption processes.

Understanding the toxic metal adsorption mechanisms as well as bond stability are important aspects for assessing the potential for immobilization in aqueous environments. The type and concentration of surface functional groups play important roles in the adsorption capacity of the biochar and in explaining the mechanism of removal of these adsorbents (WANG; WANG, 2019; WANG et al. 2019).

Techniques such as scanning electron microscopy combined with energy dispersive X-ray spectroscopy (SEM-EDS), X-ray excited photoelectron spectroscopy (XPS) and X-ray absorption spectroscopy (XAS) have been used to examine the mechanisms of retention of

toxic metals in different environments and biochars (NEVIDOMSKAYA et al., 2016; WU et al., 2017).

The scanning electron image is formed by the incidence of a beam of electrons in the material, in the vacuum. The image is generated by backscattered electron emission and demonstrates compositional differences, showing the morphological characteristics of the material. The energy dispersive system (EDS), which allows the determination of the qualitative and semi-quantitative composition of the samples, with detection limit of 1%, can be coupled to the SEM and allows the surface mapping (HOLLER; SKOOG; CROUCH, 2009).

X-ray photoelectron spectroscopy (XPS) is a technique that provides information on the elemental composition, chemical state and electronic state of the elements present in the material. A typical XPS spectrum is a graph of the number of electrons detected (per unit time) (y axis) relative to the binding energy of the detected electrons (x axis). Each element produces a characteristic set of XPS peaks at characteristic binding energy values that directly identify each element that exists on the surface or on the surface of the material being analyzed. These characteristic spectral peaks correspond to the electron configuration of the electrons within the atoms (HOLLER; SKOOG; CROUCH, 2009). Peng et al. (2017), when studying the adsorption process of Cu^{2+} and Cd^{2+} by phosphoric acid-modified biochars, found that XPS adjustment results confirmed that modification by H_3PO_4 increased the number of -COOH and -OH bond on the surface of the material and that stable structures such as C=C bonds or aromatic ring structures were formed due to the breakage of unsaturated bonds during the pyrolysis process.

Techniques based on the synchrotron radiation, which is defined as an intense electromagnetic radiation produced by high energy electrons through a particle accelerator (LABORATÓRIO NACIONAL DE LUZ SÍNCROTRON, 2019), provide detailed structural information of the materials at the atomic/molecular level.

Energies of absorption edges in XAS spectra reveal the identity of the corresponding absorbing elements. Figure 3 shows a schematic illustration of X-ray absorption spectra. The structure found in the immediate neighborhood of the absorption edge is referred to as X-ray absorption near edge structure (XANES), which provides information on oxidation state. Beyond XANES, the oscillatory structure caused by the interference between the outgoing and the back-scattered photoelectron waves is referred to as extended X-ray absorption fine structure (EXAFS). Through mathematical analysis of this region, it is possible to obtain local structural information for the atom in question (WILLMOTT, 2011). For example, studies

conducted by Wu et al. (2017), using XAS, revealed that the main Pb species observed in the biochar after the adsorption process were $Pb(C_2H_3O_2)_2$, $PbSO_4$, $Pb\text{-}Al_2O_3$, and $Pb_3(PO_4)_2$.

Figure 3. Schematic illustration of X-ray absorption spectra.

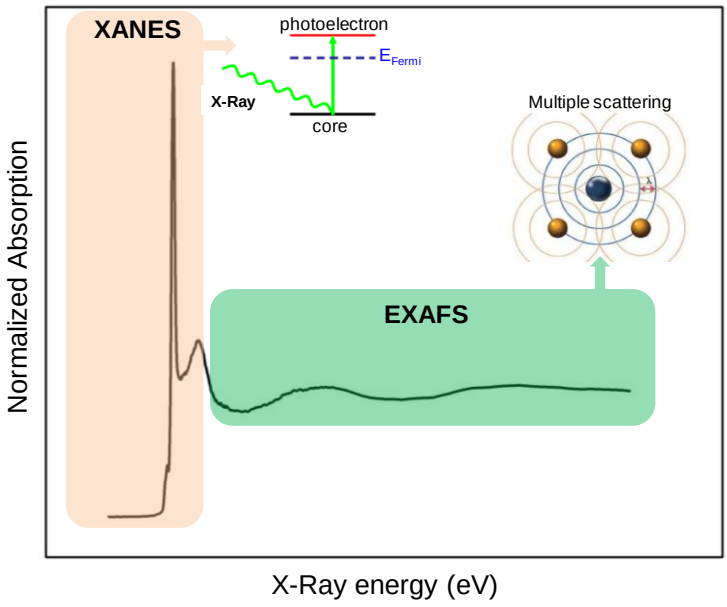

Source: from author (2019).

REFERENCES

BAIRD, C.; CANN, M. C. Química ambiental. 4. ed. Porto Alegre, RS: Bookman, 2011.

BANDOSZ, T. J. Activated **carbon surfaces in environmental remediation**. 7. ed., interface science and technology. Elsevier Academic Press, 2006.

BOLAN, N.S. et al. Uses and management of poultry litter. **Poultry Science Journal**, v. 66, 2010.

BRASSARD, P.; GODBOUT, S., RAGHAVAN, V. Pyrolysis in auger reactors for biochar and bio-oil production: A review. **Biosystems engineering**, v. 161, p. 80-92, 2017.

CAO, X. et al. Dairy-manure derived biochar effectively sorbs lead and atrazine. **Environmental Science & Technology**, v. 43, p. 3285–91, 2009.

CHEN, Z. et al. Removal of Cd and Pb with biochar made from dairy manure at low temperature. **Journal of Integrative Agriculture,** v. 18, p. 201-210, 2019.

CLARK, S. C. et al. Effluent Gas Flux Characterization during Pyrolysis of Chicken Manure. **ACS Sustainable Chemistry & Engineering**, v. 5, p. 7568–7575, 2017.

DALÓLIO, F. S. et al. Poultry litter as biomass energy: A review and future perspectives. **Renewable & Sustainable Energy Reviews,** v. 76, p. 941-949, 2017.

EMPRESA BRASILEIRA DE PESQUISA AGROPECUÁRIA, Embrapa. Suínos e Aves, Estatísticas 2018. https://www.embrapa.br/suinos-e-aves/cias/estatisticas, acessado em 9 de Julho de 2019.

GUIZANI, C. et al. The Heat Treatment Severity Index: A new metric correlated to the properties of biochars obtained from entrained flow pyrolysis of biomass. **Fuel,** v. 244, p. 61-68, 2019.

HAHN, L. et al. Persistence of pathogens and the salinomycin antibiotic in composting piles of poultry litter. **Archivos de zootecnia**, v. 61, p. 279–85, 2012

HOLLER, F. J.; SKOOG, D. A.; CROUCH, S. R. Princípios de análise instrumental. 6. ed. Porto Alegre, RS: Bookman, 2009. vii, 1055 p.

INYANG, M. I. et al. Removal of heavy metals from aqueous solution by biochars derived from anaerobically digested biomass. **Bioresource Technology**, v. 110, p. 50-56, 2012.

INYANG, M. I. et al. A review of biochar as a low-cost adsorbent for aqueous heavy metal removal. **Critical Reviews in Environmental Science and Technology**, v. 46, p. 406–33, 2016.

JAZINI, R.; SOLEIMANI, M.; MIRGHAFFARI, N. Characterization of barley straw biochar produced in various temperatures and its effect on lead and cadmium removal from aqueous solutions. **Water and Environment Journal,** v. 32, p. 125–133, 2018.

KABATA-PENDIAS, A. **Trace Elements in Soils and Plants**, 4. ed., CRC Press, 2011.

LABORATÓRIO NACIONAL DE LUZ SÍNCROTRON, LNLS, Campinas, SP. https://www.lnls.cnpem.br/o-lnls/sobre/, acessado em 10 de Julho de 2019.

LEE, M.; PARK, J. H.; CHUNG, J. W. Comparison of the lead and copper adsorption capacities of plant source materials and their biochars. **Journal of Environmental Management,** v. 236, p. 118-124, 2019.

LU, H. et al. Relative distribution of Pb^{2+} sorption mechanisms by sludge-derived biochar. **Water Resource,** v. 46, p. 854–62, 2012.

LUSTOSA FILHO, J. F. et al. Co-Pyrolysis of Poultry Litter and Phosphate and Magnesium Generates Alternative Slow-Release Fertilizer Suitable for Tropical Soils. **ACS Sustainable Chemistry & Engineering,** v. 10, p. 9043–9052, 2017.

MINISTÉRIO DA AGRICULTURA, PECUÁRIA E ABASTECIMENTO. INSTRUÇÃO NORMATIVA nº 8, de 25 de Março de 2004. Disponível em: http://sistemasweb.agricultura.gov.br/sislegis/action/detalhaAto.do?method=visualizarAtoPortalMapa&chave=178957228. Acesso em 24 de novembro de 2017.

NAEEM, M.A. et al. Combined Application of Biochar with Compost and Fertilizer Improves Soil Properties and Grain Yield of Maize. **Journal of Plant Nutrition**, p. 1532-408, 2017.

NAGAJYOTI, P. C.; LEE, K. D.; SREEKANTH, T. V. M. Heavy metals, occurrence and toxicity for plants: a review, **Environmental Chemistry Letters**, v. 8, p. 199–216, 2010.

NEVIDOMSKAYA, D.G. et al. Comprehensive study of Pb (II) speciation in soil by X-ray absorption spectroscopy (XANES and EXAFS) and sequential fractionation. **Journal of Soils and Sediments**, v. 16, p. 1183–1192, 2016.

NETHERWAY, P. et al. Phosphorus-Rich Biochars Can Transform Lead in an Urban Contaminated Soil. **Journal of Environmental Quality**, v. 48, p. 1091-1099, 2019.

PENG, H. et al. Enhanced adsorption of Cu(II) and Cd(II) by phosphoric acid-modified biochars, **Environmental Pollution**, v. 229, p. 846-853, 2017.

PREMARATHNA, K. S. D. et al. Biochar-based engineered composites for sorptive decontamination of water: A review. **Chemical Engineering Journal,** v. 372, p. 536-550, 2019.

QAMBRANI, N. A. et al. Biochar properties and eco-friendly applications for climate change mitigation, waste management, and wastewater treatment: A review. **Renewable & Sustainable Energy Reviews**, v. 79, p. 255–273, 2017.

SHAKYA, A.; AGARWAL, T. Poultry Litter Biochar: An Approach towards Poultry Litter Management – A Review. **International Journal of Current Microbiology and Applied Sciences**, v. 6, p. 2657-2668, 2017.

SHRIVER, D. F.; ATKINS, P. W. Química inorgânica. 4. ed. Porto Alegre, RS: Bookman, 2008.

SONG, W.; GUO, M. Quality variations of poultry litter biochar generated at different pyrolysis temperatures. **Journal of Analytical and Applied Pyrolysis**,v. 94, p. 138–45, 2012

TIAN, G.; WANG, W.; ZONG, L.; WANG. A. MgO/palygorskite adsorbent derived from natural Mg-rich brine and palygorskite for high-efficient removal of Cd(II) and Zn(II) ions. **Journal of Environmental Chemical Engineering**, v. 5, p. 1027–1036, 2017.

TRIPATHI, M.; SAHU, J. N.; GANESAN, P. Effect of process parameters on production of biochar from biomass waste through pyrolysis: A review. **Renewable and Sustainable Energy Reviews**, New York, v. 55, p. 467-481, 2016.

WANG, L. et al. Mechanisms and reutilization of modified biochar used for removal of heavy metals from wastewater: A review. **Science of the Total Environment**, v. 668, p. 1298-1309, 2019.

WANG , J.; WANG. S. Preparation, modification and environmental application of biochar: A review. **Journal of Cleaner Production**, v. 227, p. 1002-1022, 2019.

WILLMOTT, P. An Introduction to Synchrotron Radiation: Techniques and Applications. 1st ed, John Wiley & Sons, 2011.

WU, W. et al. Unraveling sorption of lead in aqueous solutions by chemically modified biochar derived from coconut fiber: a microscopic and spectroscopic investigation. **Science of the Total Environment**, v. 576, p. 766-774, 2017.

YOUNG, R.A. Toxicity Profiles: Toxicity Summary for Cadmium, Risk Assessment Information System, **RAIS**, University of Tennessee, 2005.

PART TWO

ARTICLE 1: CADMIUM BINDING MECHANISMS AND ADSORPTION CAPACITY BY NOVEL PHOSPHORUS/MAGNESIUM-ENGINEERED BIOCHARS

Published at Science of the Total Environment - Journal – Elsevier
(DOI https://doi.org/10.1016/j.scitotenv.2019.03.437)

Evanise Silva Penido[a], Leônidas Carrijo Azevedo Melo[b], Luiz Roberto Guimarães Guilherme[b], and Maria Lucia Bianchi[a]*

[a]Federal University of Lavras, Department of Chemistry, 3037, 37200000, Lavras, Minas Gerais, Brazil.
[b]Federal University of Lavras, Department of Soil Science, 3037, 37200000, Lavras, Minas Gerais, Brazil.

[*]Corresponding author:

Maria Lucia Bianchi
Department of Chemistry
Federal University of Lavras
Lavras, Minas Gerais, Brazil
e-mail: bianchi@dqi.ufla.br, +55 35 3829 1888

Abstract

Novel phosphorus/magnesium-engineered biochars were prepared from poultry litter and tested for their Cd^{2+} retention capacity, unraveling the adsorption mechanisms. Batch experiments were conducted to evaluate the adsorption ability of Cd^{2+} by biochars and a wide range of characterization techniques were used: scanning electron microscopy with energy-dispersive X-ray spectroscopy, Fourier transform infrared spectroscopy, surface area and pore volume, and X-ray photoelectron spectroscopy. Results showed that, in general, Cd^{2+} removal did not drastically change with initial pH variation and was relatively fast (up to 3 h); the pseudo-second-order kinetic model provided slightly better fitting to the data. Cadmium adsorption capacities of the P/Mg-engineered biochars were much higher than that of the unmodified biochar (up to 113.9 mg g^{-1}), following the SIPS isotherm model. The surfaces of the biochars contain a rich variety of oxygen-containing functional groups as well as phosphate groups. Since the specific surface areas of the biochars are considered low (up to 25.19 m^2 g^{-1}), surface groups contributed more to Cd^{2+} retention. Biochars can be represented by type II isotherms with significant type H3 hysteresis patterns, which suggest the presence of asymmetrically slit-shaped pores. Complexation and precipitation were the predominant adsorption mechanisms. Thus, P/Mg-engineered biochars produced from poultry litter are considered effective and eco-friendly adsorbents for Cd^{2+} removal from aqueous medium, especially PLB-H_3PO_4-MgO, which is produced from low-cost materials.

Keywords: poultry litter, co-pyrolysis, contamination, surface functional groups.

Graphical abstract

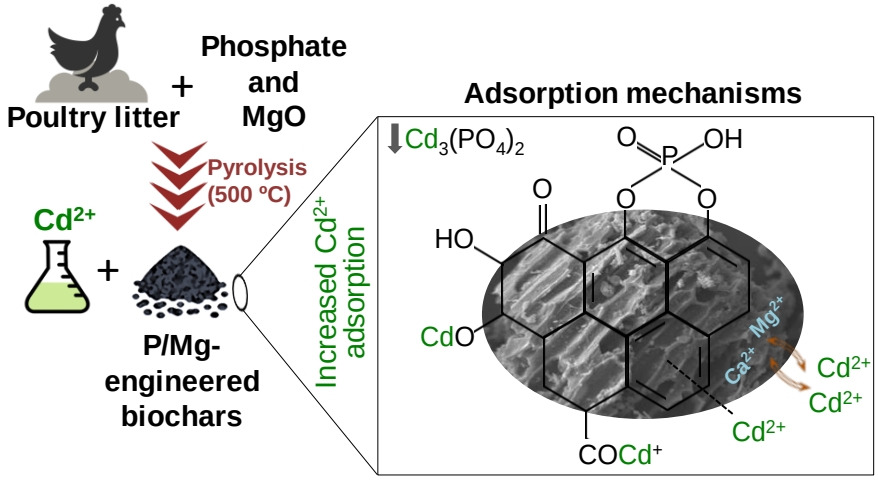

Highlights

- Novel phosphorous/magnesium-engineered biochars were prepared.
- Cd^{2+} retentions by the engineered biochars were higher than the unmodified biochar.
- Surface functional groups contributed more to Cd^{2+} retention.
- Complexation and precipitation were the predominant adsorption mechanisms.

1. Introduction

Heavy metals have been discharged into the environment worldwide, resulting in pollution of soils and water bodies. Cadmium (Cd) is one of the most challenging heavy metals due to its high toxicity and easy transfer from soils to plants, reaching also other living organisms (Kabata-Pendias, 2011). Adsorption is considered a cost-effective technique to remove heavy metals from aqueous medium or for immobilization in the soil. Lately, there has been an increasingly interest in the development of low-cost adsorbents to remove and immobilize pollutants from contaminated media (Karunanayake et al., 2018; Demey et al., 2018; Yu et al., 2018). In this regard, biochar, which is the solid product obtained from thermal treatment of any biomass in the absence or under low oxygen contents, has been widely studied (Tan et al., 2017).

Biochars present various eco-friendly applications and are considered excellent adsorbents for both organic (Zeng et al., 2018) and inorganic contaminants due to their porous structure, surface area, and high functionality (Qambrani et al., 2017). The adsorption capacity of heavy metal ions is dependent on the surface chemistry of the biochar and can occur via: (i) ion-exchange; (ii) metal−ligand complexation; (iii) cation-π bonding; and, (iv) surface (co)precipitation (Lian et al., 2017). Since surface physicochemical properties are the main factors that affect adsorption performances (Zhou et al., 2018), modifications on biochar surfaces have been studied in recent years. Surface functionalization can be achieved by a variety of approaches aiming to create functional groups, pore structures, and surface active sites in order to improve the ability of biochars to adsorb a range of contaminants from aqueous solutions (Tan et al., 2016; Tan et al., 2017). For instance, biochar surface functionalization using phosphorus (P) compounds is an effective method to increase biochar affinity for heavy metals (Peng et al., 2017; Chen et al., 2018a).

Several studies have shown that the addition of phosphate compounds to the biomass prior to pyrolysis can increase the yield, as well as the chemical, biological, and thermal stability of biochars, while reducing carbon losses during the heat treatment (Zhao et al., 2016; Xu et al., 2017; Carneiro et al., 2018). Moreover, Zhao et al. (2017) found that the co-pyrolysis of biomass with phosphoric acid generated thermally stable phosphorus complexes, such as $C{-}O{-}PO_3$ and $(CO)_2PO_2$, on the surface of biochar. Magnesium oxide (MgO) is also used as an active component to improve the adsorption performance of heavy metal ions due to increases in surface area and oxygen-containing groups (Cai et al., 2017; Tian et al. 2017). Carneiro et al. (2018) observed that the impregnation of MgO and H_3PO_4 increased the surface area of the prepared biochar, while Lustosa Filho et al. (2017) found an increase in pH and CEC in biochars enriched with MgO plus phosphate sources (TSP and H_3PO_4) when compared with the same biochars enriched only with phosphate sources. Thus, these changes in the characteristics of biochar caused by MgO and phosphate additions make these materials promising for Cd^{2+} adsorption. However, studies exploring the potential adsorption capacity as well as the mechanisms governing Cd adsorption on such P/Mg-engineered biochars, especially considering the desorption characteristics, are still lacking.

Among the feedstock for biochar production, poultry litter is of special interest due to the growing global production of broiler meat in recent years, which generates large amounts of residues. Brazil is the second world broiler producer, generating nearly 8-10 million tons per year (Dalólio et al., 2017). However, the disposal of raw poultry litter in the environment is a concern, which requires increasingly sustainable alternatives for its reuse. Among the

options, pyrolysis of poultry litter to produce biochar can be an economically sustainable alternative, including its use as an adsorbent for heavy metals. For example, Idrees et al. (2016) found a Cd^{2+} adsorption capacity as high as 90.1 mg g^{-1} in poultry manure biochar, while Qi et al. (2017) found that chicken litter biochar pyrolysed at 550 ºC retained 48.5 mg g^{-1} of Cd^{2+}, exhibiting an increased retention capacity up to 60.9 mg g^{-1} of Cd^{2+}, after a further combustion at 375 °C for 24 h to remove the labile non-carbonized.

Despite many studies have been performed on biochar and Cd^{2+} adsorption from aqueous solution, studies exploring in details the retention mechanisms using novel engineered biochars are of great importance. Therefore, the objective of this work was to investigate the Cd^{2+} retention potential of P/Mg-engineered biochars through a batch adsorption assay, exploring their physicochemical properties in order to unravel and quantify the adsorption mechanisms.

2. Material and Methods

2.1. Poultry litter sampling and biochar preparation

The poultry litter (PL) used in this study was collected from a farm in the state of Minas Gerais, Brazil (915 m altitude, 21°13′34″ S and 44°58′31″ W). Poultry litter samples were air-dried at room temperature and ground to pass through a 20-mesh sieve (1.00 mm). Subsequently, separate aliquots of PL were mixed with the following P compounds: monoammonium phosphate - MAP ($NH_4H_2PO_4$), triple superphosphate - TSP [$Ca(H_2PO_4)_2$], and phosphoric acid (H_3PO_4). Magnesium oxide (MgO) was added aiming to reduce the residual acidity of the P compounds and also to increase the surface area of the biochars. Phosphate sources and MgO were mixed to achieve a P/Mg molar ratio of 1:1, and the ratio of poultry litter/phosphate source was 1:0.5 (w/w). The pretreated samples were pyrolysed by raising the temperature up to 500 °C at a heating rate of 10 °C min^{-1}, maintaining the target temperature for 2 h. Detailed information concerning the preparation of the biochars can be found elsewhere (Lustosa Filho et al., 2017). This pyrolysis temperature was chosen aiming to maximize the yield and to increase carbon stabilization of the biochar (Zhao et al., 2016; Wei et al., 2019), as well as to preserve the surface oxygen functional groups (Chen et al., 2019). The produced biochars were identified as follows: PLB (poultry litter biochar), PLB-MAP-MgO, PLB-H_3PO_4-MgO, and PLB-TSP-MgO.

2.2. Blocking of carboxyl and hydroxyl groups

In order to investigate the role of carboxyl and hydroxyl groups on Cd^{2+} complexation, the produced P/Mg-engineered biochars were chemically modified to be further used in Cd^{2+} removal. The modification of carboxyl groups was carried out by reaction with methanol and concentrated HCl, resulting in esterification of the carboxylic groups. As for hydroxyl groups, biochars were treated with formaldehyde. Both reactions followed the methodology described by Kousha et al. (2012).

2.3. Batch adsorption/desorption experiments

Adsorption studies were conducted to investigate the kinetic and equilibrium parameters of Cd^{2+} in solution. Cadmium solutions were prepared by dissolving $Cd(NO_3)_2$ in 0.01 mol L^{-1} $NaNO_3$. Dilutions were performed from the stock solution to the required concentrations of each test prior to use.

In order to investigate the influence of pH on the adsorption process, the initial pH of the solution was adjusted to the desired values in the range of 2 to 10 using either 0.1 mol L^{-1} NaOH or 0.1 mol L^{-1} HCl solutions. This test was performed using 0.04 g of each biochar and 10 mL of a solution of 300 mg L^{-1} Cd^{2+} at 25 °C with 24 h of stirring. To evaluate adsorption kinetics, 0.04 g of each biochar were mixed with 10 mL of a solution containing 300 mg L^{-1} of Cd^{2+} at initial pH 5.6 (natural pH of the Cd solution). Solutions were stirred and filtered at predetermined regular time intervals (5, 10, 15, 30, 60, 300, 720, and 1440 min). For the isotherm study, 4.0 g L^{-1} of each biochar were added to Cd^{2+} solutions with initial concentrations ranging from 20 to 800 mg L^{-1}. The extracts were quantified by atomic absorption spectroscopy with air-acetylene flame (FAAS), using Perkin Elmer Analyst 800 equipment.

For the desorption tests, larger mass portions of biochars were used firstly in adsorption tests, as previously described. After filtering in paper filters, samples were oven dried (60 °C) for 24 hours. Three different desorption solutions were used: 0.01 mol L^{-1} $CaCl_2$, 1 mol L^{-1} HCl, and 0.1 mol L^{-1} acetic acid solution by the TCLP method (USEPA, 1992), which determines the mobility of an analyte in solid wastes. The desorption experiments were carried out using 0.1 g of Cd-loaded biochar in 10 mL of each desorption solution, with 24 hours of stirring. The extracts were analyzed by ICP-OES for Cd.

To investigate the influence of ion exchange capacity and precipitation on Cd^{2+} adsorption, 0.04 g of each biochar were placed in contact with 10 mL of 250 mg L^{-1} of Cd^{2+} at pH 5.6, under stirring for 24 h. Control samples without Cd^{2+} were prepared under the same conditions. The extracts were analyzed by ICP-OES for Ca, Mg, P, and Cd.

The studied biochars and biochars treated to block carboxyl and hydroxyl groups, as previously described, were placed in contact with a 250 mg L^{-1} Cd^{2+} solution at a dose of 4 g L^{-1} in order to evaluate the role of these functional groups on Cd^{2+} retention.

For all tests, after the adsorption equilibrium was reached, the solutions were separated from the solid material by membrane filtration (0.45-µm Millipore pore size). Control tests were performed in parallel, without addition of biochars. Each trial was performed in triplicate and the mean values were considered.

2.4. Isotherm and kinetics models

The amount of Cd^{2+} adsorbed per unit mass of biochar was calculated according to Equation 1:

$$q_{eq} = \frac{(C_0 - C_{eq}) \times V}{m} \quad (1)$$

in which qe (mg g-1) is the amount of Cd^{2+} adsorbed on biochar, C_0 and C_{eq} (mg L^{-1}) are the initial and equilibrium Cd^{2+} concentrations in the aqueous solution, V (L) is the volume of the solution, and m (g) is the mass of biochar.

Isotherm models are widely employed for fitting the data. The Langmuir (1916) and Freundlich (1906) equations are the most widely used to examine the relationship between the amount adsorbed (q_e) and the aqueous concentration C_e at equilibrium.

The Langmuir equation may be written as:

$$q_e = \frac{Q^0 b C_e}{1 + b C_e} \quad (2)$$

in which C_e is the equilibrium concentration (mg L^{-1}), q_e the amount of metal ion adsorbed (mg g^{-1}), Q_0 the amount of metal ion adsorbed for a complete monolayer (mg g^{-1}), b is the sorption equilibrium constant.

The Freundlich equation may be written as:

$$q_e = K_F C_e^{1/n} \quad (3)$$

The K_F and 1/n of the Freundlich model are the constants indicative of the relative adsorption capacity of the adsorbent (mg g^{-1}) and the intensity of the adsorption, respectively.

By studying the distribution of adsorption energies of the sites of an adsorbent surface, Robert Sips (1948) proposed an empirical isotherm equation, expressed as:

$$q_e = Q^0 \frac{kC_e^{n_s}}{1+kC_e^{n_s}} \quad (4)$$

in which ns is the Sips constant.

As for kinetics, pseudo first-order (Equation 5) and pseudo second-order (Equation 6) models were used for assessing the reaction order of Cd^{2+} adsorption onto biochars.

$$Q_t = q_e(1 - e^{-k_1 t}) \quad (5)$$

$$Q_t = \frac{Q_t k_2 t}{1+q_e k_2 t} \quad (6)$$

in which Q_t is the amount of Cd^{2+} adsorbed (mg g^{-1}) at time t, q_e is the amount of Cd^{2+} adsorbed (mg g^{-1}) at equilibrium time, and k_1 (h^{-1}) and k_2 (g mg^{-1} h^{-1}) are the rate constants of the pseudo first-order equation and pseudo second-order equation, respectively (Simonin, 2016).

2.5 Biochar characterizations

The pH drift method, developed for activated carbons, was used to determine the point of zero charge (pHPZC), as described in Bayazit and Kerlez (2014). Scanning electron microscopy/energy dispersive X-ray spectroscopy (Carl Zeiss mod. EVO 50/IXRF Systems mod. 500 Digital Processing) was used to characterize the chemical composition and structural morphologies of the materials before and after Cd^{2+} adsorption. Biochars' specific surface areas (BET method) and pore volumes (BJH method) were calculated by nitrogen (N2) adsorption/desorption analysis carried out at 77 K, with cold free space of 50.7 cm^3, equilibration interval of 10 s, and automatic degas (Quantachrome Instruments). Fourier-transform infrared spectroscopy (Varian/mod. 660 IR) was used to identify the functional groups on biochars' surfaces before and after Cd^{2+} adsorption. The spectra were investigated in the 4000-400 cm^{-1} region under a 4 cm^{-1} resolution, with 16 scans. X-ray photoelectron spectroscopy (UNI-SPECS UHV) was performed to analyze the composition and chemical state of the surface elements of the materials using a k alpha Mg source, hv 1253.6eV before and after Cd^{2+} adsorption.

3. Results and Discussion

Data on physical and chemical properties of the studied biochars can be found in our previous study (Lustosa Filho et al. 2017). Briefly, the pH value of unmodified PLB was 11.1, while for PLB-MAP-MgO, PLB-H_3PO_4-MgO and PLB-TSP-MgO the pH values were 6.9, 9.1, and 6.1, respectively. The C content of the biochars was relatively low (ranging from 19.0% to 31.4%), which may be explained by the dilution effect of mixing inorganic sources with poultry litter. Total P contents in the biochars ranged from 24.4 for PLB to 162 g kg^{-1} for PLB-H_3PO_4-MgO, which shows that P compounds are retained in the biochar after pyrolysis at 500 ºC.

3.1 Batch adsorption experiments

Preliminary experiments were conducted to determine the optimum pH for Cd^{2+} retention by the biochars (Fig. 1). Cadmium removal from solution increased as the initial pH increased from 2 to 9 for PLB. The remarkably low adsorption capacity at pH 2.0 for PLB can be related to the linkage of H^+ with oxygen-containing functional groups that could prevent access for metal ions, since the equilibrium pH was also very low (Fig. 1A). Moreover, in lower pH medium, PLB has the predominance of positive charges on its surface due to its high pH_{PZC} = 7.0, and the high electrostatic repelling forces inhibits the contact of Cd^{2+} and the biochar. The pH_{PZC} values for PLB-MAP-MgO, PLB-H_3PO_4-MgO, and PLB-TSP-MgO are 6.1, 5.5, and 6.2, respectively.

As for the P/Mg-engineered biochars, Cd^{2+} removal did not drastically change with initial pH variation, especially for PLB-H_3PO_4-MgO and PLB-TSP-MgO (Fig. 1A). The equilibrium pH values of these biochars were nearly constant (pH ~ 4), indicating that Cd^{2+} adsorption takes place in a wide range of pH values (Fig. 1B). Previous studies have shown that a pH of 5.0-6.0 was optimum for Cd^{2+} adsorption (Karunanayake et al., 2018; Wang et al. 2018). Thus, all subsequent adsorption experiments in this study were conducted at pH 5.6, which is the natural pH of the prepared Cd^{2+} solution.

The removal processes of Cd^{2+} were relatively fast, reaching equilibrium after 1.15 h of contact for PLB-H_3PO_4-MgO and 3 h for PLB-MAP-MgO and PLB-TSP-MgO (Fig. 2). The initial pH values of the solutions were ~5.6 and the equilibrium pH values after adsorption were similar to those studied for the pH effect (Fig. 1B) for each collection interval at pH 5. In earlier stages, there is great abundance of vacant sites on the biochar surface,

whereas as adsorption continued, a progressive saturation of these active sites might have occurred with time.

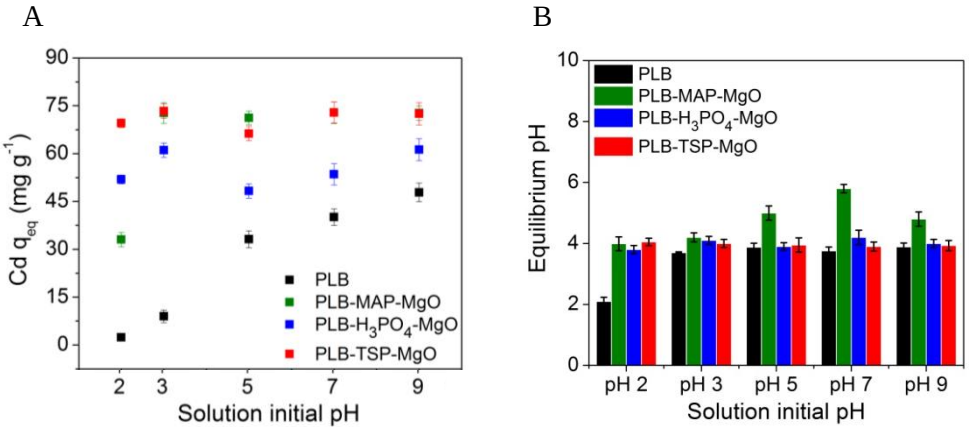

Fig. 1. Effect of pH on Cd^{2+} retention (mg g^{-1}) by P/Mg-engineered biochars (A) and solution equilibrium pH after 24 h of stirring (B). Conditions: biochar dose = 4 g L^{-1}; initial concentration = 300 mg L^{-1} Cd^{2+}.

First-order and second-order kinetic models were fit to the experimental data obtained from batch experiments (Table 1). The pseudo-second-order kinetic model provided slightly better fitting for PLB and PLB-H_3PO_4-MgO. This indicates that the reaction rate of Cd^{2+} adsorption depended more on the number of active sites and the rate-limiting step may be chemical adsorption, through sharing or exchange of electrons. As for PLB-MAP-MgO and PLB-TSP-MgO, lower constant rates were observed (Table 1) with slightly higher R^2 values for pseudo-first order, which indicates that physisorption plays an important role on Cd^{2+} retention onto those biochars (Jazini et al., 2018; Wei et al., 2018).

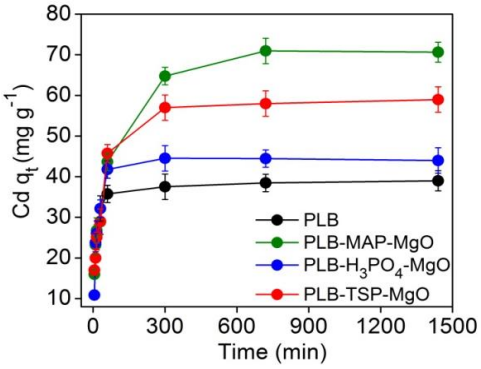

Fig. 2. Effect of contact time on Cd^{2+} retention onto P/Mg-engineered biochars at initial pH of 5.6, using a biochar dose of 4 g L^{-1} and solution of 300 mg L^{-1} of Cd^{2+}.

The adsorption isotherms showed maximum adsorption capacities in the following order: PLB < PLB-MAP-MgO < PLB-TSP-MgO < PLB-H_3PO_4-MgO (Table 2). The adsorption isotherms of the biochars can be found in the supplementary material. Cadmium adsorption capacities of the P/Mg-engineered biochars were much higher than that of the unmodified biochar, confirming that P and Mg compounds contributed greatly to the adsorption ability of the sorbents.

Analysis of the regression coefficients (R^2) showed that Cd^{2+} adsorption by biochars fitted well to the SIPS model (Table 2), which is used for predicting heterogeneous adsorption systems. When the metal concentrations are low, SIPS follows the Freundlich isotherm model, while at high metal concentrations, it approaches the Langmuir isotherm model (Foo and Hameed, 2010). The 1/n values from the Freundlich model were all less than one, indicating that Cd^{2+} adsorption was viable for all biochars. Thus, Cd^{2+} adsorption is a complex process where there was not only monolayer adsorption, but also heterogeneous adsorption occurring (Shen et al., 2017).

Table 1: Kinetic parameters of pseudo-first order and pseudo-second order.

Biochar	pseudo-first order		pseudo-second order	
	k_1	R^2	k_2	R^2
PLB	-2.128	0.933	0.130	0.987
PLB -MAP-MgO	-0.715	0.958	0.085	0.948
PLB -H_3PO_4-MgO	-2.767	0.979	0.111	0.999
PLB -TSP-MgO	-1.437	0.964	0.062	0.925

k_1 (h^{-1}) and k_2 (g mg^{-1} h^{-1}) is the rate constant and Q_t and q_e (mg g^{-1}) are the amount of adsorbate adsorbed per unit mass at time t (h) and at the equilibrium state, respectively.

Table 2. Langmuir, Freundlich, and SIPS isotherm parameters for Cd^{2+} adsorption on P/Mg-engineered biochars.

Biochar	Isotherm models								
	Langmuir			Freundlich			SIPS		
	Q^0	b	R^2	K_F	1/n	R^2	Q^0	n_s	R^2
PLB	49.09	0.01	0.857	4.59	0.35	0.981	52.05	0.354	0.975
PLB -MAP-MgO	72.34	0.12	0.958	17.69	0.24	0.800	69.01	0.998	0.955
PLB -H_3PO_4-MgO	84.41	0.02	0.962	10.26	0.35	0.962	113.9	0.631	0.981
PLB -TSP-MgO	75.48	0.04	0.952	12.39	0.30	0.935	93.58	0.644	0.970

Qm is the maximum adsorption capacity (mg g^{-1}), q_e adsorption capacity at equilibrium (mg g^{-1}), C_e is the equilibrium concentration (mg L^{-1}), K_F is the Freundlich affinity coefficient, and n is the Freundlich nonlinearity factor, and ns is the Sips constant.

3.2 Desorption experiments

During the adsorption process, Cd^{2+} in solution may be retained on the biochar by cation exchange reactions. Electrostatically adsorbed ions are easily desorbed in an unbuffered neutral salt solution (Jazini et al., 2018). The extraction using 0.01 mol L^{-1} $CaCl_2$ desorbed only up to 1.6% of the adsorbed Cd^{2+} (Fig. 3). Desorption values were higher for PLB-MAP-MgO and PLB-TSP-MgO, indicating that Cd^{2+} is less strongly retained on these biochars when compared with PLB and PLB-H_3PO_4-MgO. This same pattern was observed for HCl extraction, although much larger amounts of Cd^{2+} were desorbed due to the strong acid solution (1 mol L^{-1} HCl). On the other hand, TCLP extraction for Cd^{2+} was higher for PLB than for the P/Mg engineered biochars, which shows a lower leaching potential in these materials as compared with pristine biochar (PLB). Liang et al. (2014) also found a reduced Cd^{2+} extraction by the TCLP solution in a Cd-contaminated soil amended with P-rich biochar and phosphate. Nevertheless, none of the solutions extracted 100% of Cd^{2+}, suggesting the occurrence of non-electrostatic adsorption of Cd^{2+} (Wei et al., 2018).

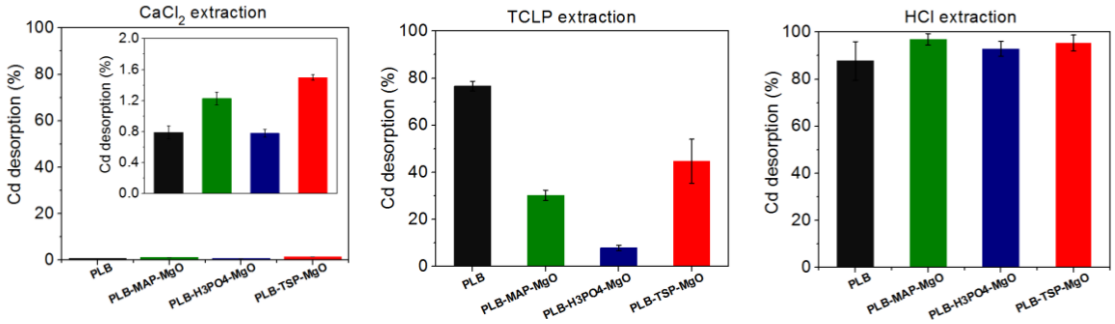

Fig. 3. Cadmium desorption (%) using different extractants. Fig. 3. Cadmium desorption (%) using different extractants. Conditions: 0.01 mol L^{-1} $CaCl_2$, 1 mol L^{-1} HCl, and 0.1 mol L^{-1} acetic acid; 0.1 g of Cd-loaded biochar and 10 mL of solution.

3.3 Biochar characterization

SEM images prior to adsorption and EDX elemental maps of Cd-loaded biochars are shown in Fig. 4. The surface of the raw biochar was uneven and smooth. As for the engineered biochars, more particles emerged on surface and numerous honeycomb porous structures appeared, especially for PLB-MAP-MgO and PLB-TSP-MgO. Results from the EDX data indicated that O, P, Mg, Ca, and C were the major elements in the biochars. There is a high correlation between adsorbed Cd^{2+} and P and O, indicating that Cd^{2+} adsorption

might have occurred predominantly to phosphate and oxygen functional groups, as further discussed.

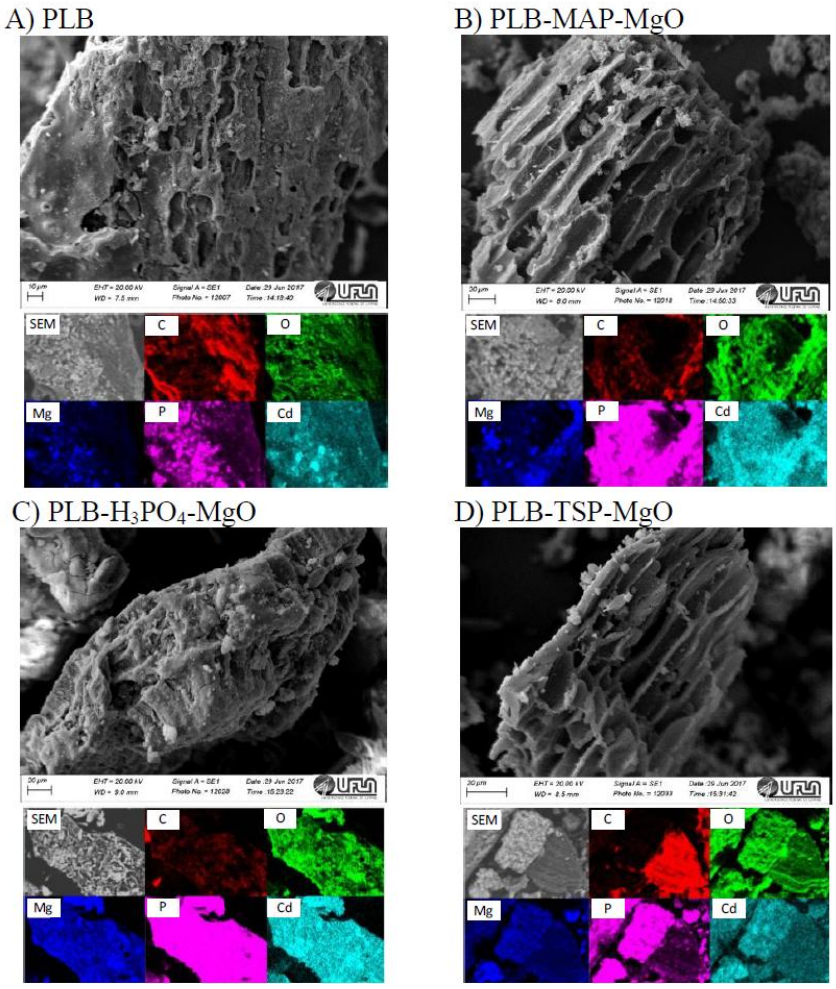

Fig. 4. SEM micrographs and EDX elemental maps of P/Mg-engineered biochars.

The specific surface areas of biochars are considered low, suggesting that pores can be partially closed and prevent easy access to adsorption (Fig. 5). The highest surface area was found for PLB-TSP-MgO (25.19 $m^2\ g^{-1}$), followed by PLB-MAP-MgO (23.49 $m^2\ g^{-1}$), which was nearly four times higher than for PLB (6.08 $m^2\ g^{-1}$). Treatment with H_3PO_4 and MgO did not expressively increase the surface area, but there was an increase in total pore volume when compared with PLB (Fig. 5). Thus, the maximum adsorption capacity of PLB-H_3PO_4-MgO (Table 2) was likely not controlled by surface area and thus, other features, such as surface groups, might have a greater contribution to Cd^{2+} retention. For example, Zhou et al. (2018) demonstrated that a Fe-Mn binary oxide–biochar composite is an excellent adsorbent for Cd^{2+} retention (101.0 mg g^{-1}) even though the BET surface area of the material was 71.64 ± 0.17 $m^2\ g^{-1}$. Activated carbons with surface area of the order of 1500 $m^2\ g^{-1}$ are described in the literature (Silva et al., 2018). However, the chemical activation process of carbons often

requires a washing step to clean the pores and remove the activation agent (Liou, 2010). In this study, surface functionalization with Mg and P compounds was chosen over surface activation. Thus, there was no acid washing step after the preparation of the biochar, which could also justify the low surface area of the materials.

Phosphorus/magnesium-engineered biochars can be represented by type II isotherms (Fig. 5A), which infer that the prevailing process at low relative pressure is the formation of a monolayer of adsorbed molecules, while at high relative pressure a multilayer adsorption takes place (Thommes et al., 2015). All samples display isotherms with significant type H3 hysteresis patterns, which suggest the presence of asymmetrically slit-shaped pores (plate-like particles) (Shen et al., 2018). The steepest slopes due to the high difference in volumes of gas adsorbed at the two last pressure points and the low hysteresis at this point (Fig. 5A) are indicative of macroporous nature, especially for PLB and PLB-H_3PO_4-MgO (Hazra et al., 2018). As for pore size distribution, the biochar samples were all heterogeneous in their surface characteristics, with high proportion of large pores. Treatment with MAP and TSP along with MgO developed mesoporosity of biochars as observed by the higher proportion of larger pores into these materials, especially for PLB-MAP-MgO (Fig. 5B). By using Raman spectroscopy, Carneiro et al. (2018) found that MgO caused an increase in the specific surface area of biochars and the occurrence of structural defects (amorphous carbon). Thus, the higher disorder in the C structure is an important characteristic of biochar to be used as an adsorbent, since it can increase the oxidation of aromatic rings, which gives rise to broken links that increase ion exchange by the chemical bond with Cd^{2+} ions present in solution.

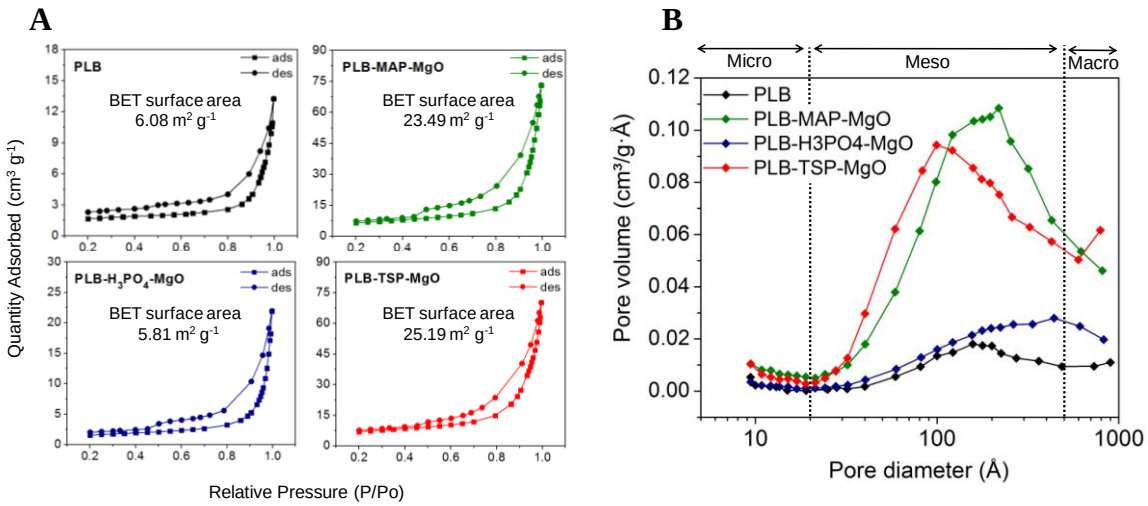

Fig. 5. Nitrogen isotherms of biochars and BET surface areas (A) and pore size distribution of biochars using dV/dlog (r) *vs* r plots (B).

FTIR spectra of biochars with and without Cd loading are shown in Fig. 6. The surfaces of the biochars contain a rich variety of oxygen-containing functional groups. Some bands can be less evident in biochar treated with P and Mg compounds due to the overlaying of these elements in the surface of the materials, as shown in the EDX mapping. Aromatic stretches (1600 and 1436 cm^{-1}) as well as C=O (1680 cm^{-1}) and O-H (1375 cm^{-1}) elongation can be observed. Peaks around 1540 cm^{-1} can be assigned to amino groups. Phosphorus stretches are found in regions below 1000 cm^{-1}, mainly P-O-P stretches of esters and pyrophosphates (Bekiaris et al., 2016; Lustosa Filho et al., 2017). Negatively charged group bands moved or changed intensity after Cd^{2+} adsorption, indicating that they were involved in the adsorption process, especially for PLB and PLB-H_3PO_4-MgO (Fig. 6). The FTIR spectra of PLB-MAP-MgO and PLB-TSP-MgO presented significantly fewer types of functional groups on their surface, suggesting that these groups do not significantly contribute to Cd^{2+} adsorption.

Biochar surfaces are electron-rich π-systems that may donate π-electrons in acid-basic Lewis reactions (Peng et al., 2017). Shifts are observed for FTIR peaks of PLB-MAP-MgO attributed to aromatic C-H at around 840 cm^{-1} and C=C at around 1600 cm^{-1}, as indicated by the arrows (Fig. 6).

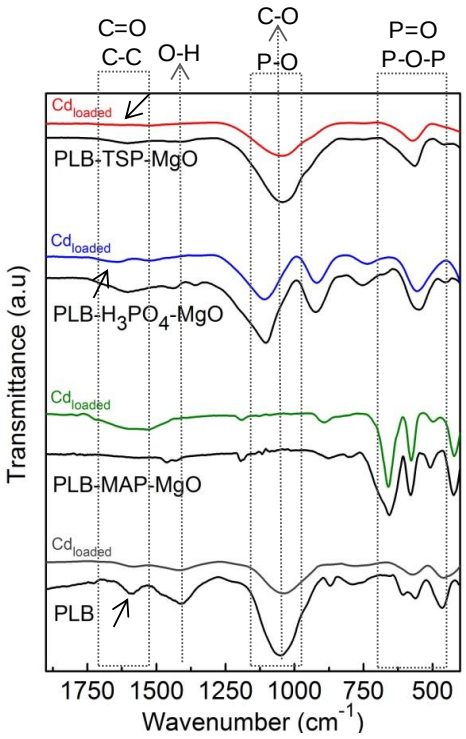

Fig. 6. FTIR spectra of biochars before and after Cd^{2+} adsorption

The distinct peaks yielded from the deconvolution of C1s, O1s, P2p, and Cd3$d_{5/2}$ XPS spectra are present in Fig. 7 for PLB-H_3PO_4-MgO. Spectra of other biochars are shown in the supplementary material. XPS-fitting results confirmed that H_3PO_4 and MgO modification increased the number of -COOH and -OH groups, which is observed by the larger and more intense peaks (increased peak area), when compared with pristine biochar (PLB) (Fig. 7A), representing oxygen increase onto the biochars' surfaces and abundant sites for Cd^{2+} chemical adsorption. For C1s, the peak centered at 285.0 eV was assigned for C-C bonds, at 286.5 eV to C-OH bonds, and at 283.0 eV to C=O. As for O1s, C-OH can be found at 532.9 (also assigned for C-O-P groups) and 533.6 eV, while non-carbonyl oxygen in carboxylic groups can be found at 534.5 eV. The carbon and oxygen functional groups shifted after Cd^{2+} adsorption, indicating that those groups play a role in the adsorption mechanism.

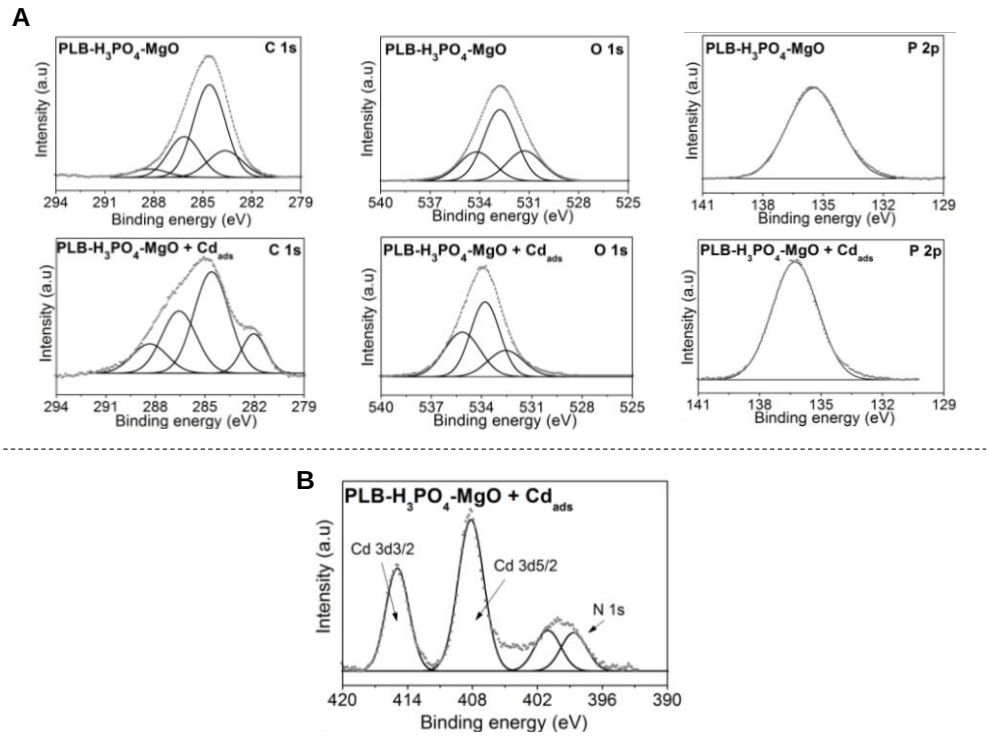

Fig. 7. XPS deconvoluted spectra of PLB-H_3PO_4-MgO before and after Cd^{2+} adsorption for C 1s, O 1s, and P 2p (A) and Cd 3d after adsorption (B).

The spectra for P2p show a signal at 133.2 eV from PO_4^{3-}. For PLB, after Cd^{2+} adsorption, the peak is slightly shifted to higher binding energy and a new peak appeared at 135.3 eV, which could correspond to P_2O_5 (NIST database). At 135.2 eV, binding energies corresponding to H_3PO_4 can be observed for PLB-MAP-MgO (Fig B. Supplementary material) and PLB-H_3PO_4-MgO (Figure 6) biochars (NIST database); after Cd^{2+} retention,

those peaks increased their intensity and shifted to higher binding energies, respectively. Cadmium loaded on biochars can be evidenced by the $Cd3d_{5/2}$ deconvoluted peak in the XPS spectra after Cd^{2+} adsorption (Fig. 7B). Bogusz et al. (2015) attributed the binding energy of approximately 406 eV in the Cd3d5/2 region to CdO.

In previous tests we observed higher adsorption of Cd^{2+} using MgO-treated samples as compared with samples without MgO (data not shown). This synergistic effect can be explained by the increase in amorphous C in the MgO-treated samples (Carneiro et al., 2018) and also due to the increased pH with the addition of MgO, since the phosphate sources (H_3PO_4 and MAP) present an acidic nature. Moreover, there is an increase of O-containing functional groups on the surface of the biochars produced by co-pyrolysis of both phosphate and MgO sources (Lustosa Filho et al., 2017).

3.4 Cation exchange and precipitation and complexation reactions

Since the P/Mg-engineered biochars have large quantities of Ca and Mg, during the adsorption process Cd^{2+} in solution may be retained on the biochar by cation exchange reactions with Ca^{2+} and Mg^{2+}. Fig. 8A shows the release of Mg^{2+} and Ca^{2+} with and without Cd^{2+} adsorption (control samples). Sample PLB-TSP-MgO presented the highest amount of Cd^{2+} adsorbed via cation exchange, with both Mg^{2+} and Ca^{2+} being released to solution, followed by PLB. This is due to the composition of these materials, which are rich in exchangeable Mg^{2+} and Ca^{2+}.

Previous studies have reported precipitation of Cd^{2+} with CO_3^{2-} and PO_4^{3-} released from biochars (Deng et al., 2018). As shown in Fig. 8B, contents of total P in solution after Cd adsorption were lower when compared with control samples (water soluble P) for all biochars, especially for PLB-MAP-MgO and PLB-H_3PO_4-MgO, possibly forming amorphous $Cd_3(PO_4)_2$.

The decrease in solution pH after Cd^{2+} adsorption (Fig. 1B) is supported by the increase of H^+ ions in solution when comparing the blank samples with the equilibrium solution after Cd^{2+} adsorption (Fig. 8C). Thus, the deprotonation of hydroxyl and carboxyl can enhance the interaction between biochar and metal ions, releasing H_3O^+ to the medium and decreasing pH (Chen et al., 2018b), as shown below:

$$-COOH + Cd^{2+} + H_2O \rightarrow -COOCd^{+} + H_3O^{+}$$

$$-OH + Cd^{2+} + H_2O \rightarrow -OCd^{+} + H_3O^{+}$$

The formation of the Cd^{2+} precipitates with alkali ions (PO_4^{3-}) from biochars can also decrease solution pH after Cd^{2+} retention.

Fig. 8D shows the influence on the adsorption efficiency by blocking of functional groups. The esterification and methylation of the functional groups decreased the percentage of Cd^{2+} removal from solution, showing the important role that –COOH and –OH play in the binding of Cd ions. PLB and PLB-H_3PO_4-MgO presented higher differences of Cd^{2+} removal when compared with PLB-MAP-MgO and PLB-TSP-MgO. This result is in accordance with those obtained by FTIR, which showed that PLB-MAP-MgO and PLB-TSP-MgO presented less oxygen functional groups on their surface. Since, as far as we know, this is the first study using this approach in Cd^{2+} adsorption using biochars, we could not compare our results with others. However, it highlights the importance of these two functional groups on Cd adsorption onto biochar surfaces.

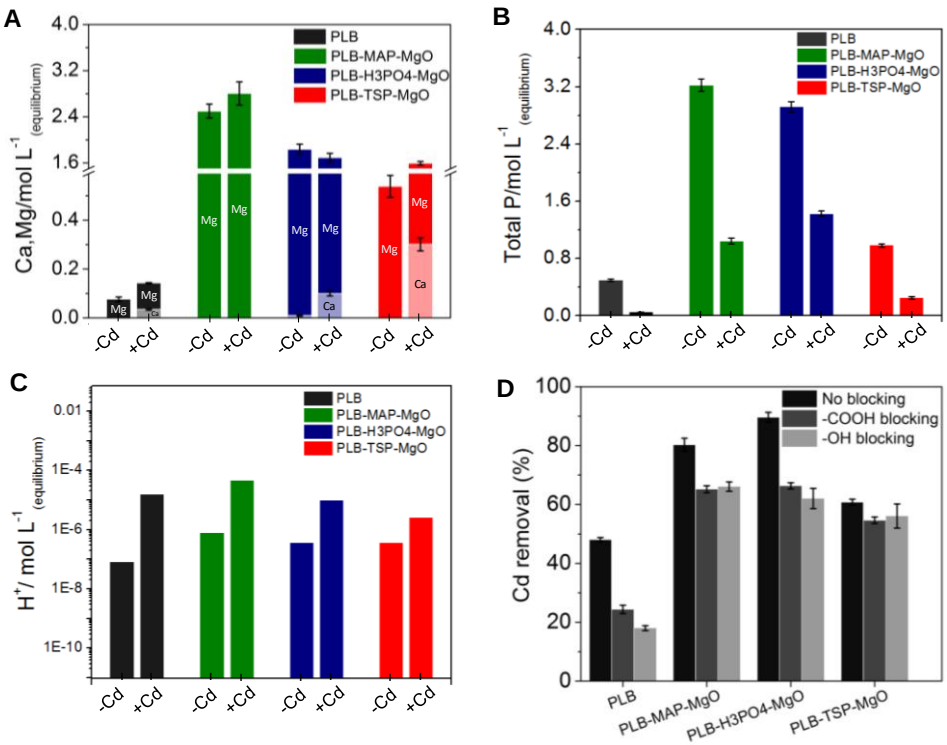

Fig. 8. (A) Contents of Ca^{2+} and Mg^{2+} in solution after Cd adsorption by Mg/P-engineered biochars. (B) Contents of total P in solution after Cd adsorption by Mg/P-engineered biochars. (C) Contents of H^+ in solution after Cd adsorption by Mg/P-engineered biochars, obtained from pH (triplicates). –Cd = blank solution; +Cd = initial Cd^{2+} of 250 mg L^{-1} at biochar doses of g L^{-1}. (D) Effect of carboxylic and hydroxyl groups on Cd removal from solution.

3.5 Comparative studies of Cd^{2+} removal by different biochars

A literature survey on the maximum adsorption capacity of Cd^{2+} and the main mechanisms governing the retention process between various adsorbents was performed (Table 3). The P/Mg-engineered biochars, especially PLB-H_3PO_4-MgO, presented higher maximum adsorption capacities when compared with the results of the most recent studies of Cd^{2+} adsorption on various types of biochars. Complexation with O-containing functional groups is the predominant mechanism of Cd^{2+} adsorption.

4. Conclusion

Phosphorus/magnesium-engineered biochars were successfully prepared by co-pyrolysis of P sources and MgO with poultry litter. The materials are considered effective and eco-friendly adsorbents since the cadmium adsorption capacities of the P/Mg-engineered biochars were much higher than that of the unmodified biochar, especially PLB-H_3PO_4-MgO, which is produced from low-cost materials.

The presence of oxygen and phosphorus functional groups on the biochars' surfaces and their shifting after Cd loading suggested that Cd^{2+} was mostly retained by surface complexation. The decrease in solution pH after adsorption as well as the decrease in the percentage of Cd^{2+} removal from solution after the esterification and methylation of the functional groups also showed the important role that –COOH and –OH play in the binding of Cd^{2+} ions. Precipitation also takes place, possibly forming amorphous $Cd_3(PO_4)_2$. Thus, complexation and precipitation were the predominant adsorption mechanisms.

This study provided basis for future research focusing on Cd-polluted wastewater remediation. It can also contribute to heavy-metal-polluted soil remediation considering engineered biochars as amendments.

Acknowledgements

The authors would like to thank the Minas Gerais State Agency for Research and Development – FAPEMIG for financial support and scholarship to the first author. This study was financed in part by the Coordenação de Aperfeiçoamento de Pessoal de Nível Superior – Brasil (CAPES) – Finance Code 001. The National Council for Scientific and Technological

Development (CNPq) are also acknowledged. LCA Melo and LRG Guilherme are Research Fellows of the National Council for Scientific and Technological Development.

Table 3: Comparison of maximum Cd^{2+} adsorption capacities and overall mechanism with other recent reported data.

Biochar	**Cd^{2+} maximum adsorption (mg g^{-1})**	**Pyrolysis temperature (°C)**	**Overall mechanism**	**Reference**
Reed biochar modified by ferrous ammonium sulfate	2.9	450	Associations with functional groups	(Cui et al., 2019)
Rice straw biochar modified with KOH	41.9	500	Surface precipitation by forming insoluble Cd compounds in alkaline condition and ion exchange	(Bashir et al., 2018)
Yak manure biochar by H_2O_2	69.1	350	Not elucidated	(Wang and Liu, 2018)
Biochar derived from lotus seedpods	51.2	600	Surface complexation, ion exchange, surface precipitation, and Cd–π interaction	(Chen et al., 2018b)
Swine manure-derived biochar	22.0	500	Precipitation and ion exchange were prominent	(Deng et al., 2018)
Chicken-manure-derived biochar	60.0	500	Complexation and precipitation were prominent	(Huang et al., 2018)
Fresh sugarcane bagasse biochar	26.8	500	Not elucidated	(Hass and Lima, 2018)
Poultry manure biochar	44.9	500	Ion exchange	(Lei et al., 2019)
Dairy manure biochar modified with NaOH	68.1	300	Precipitation as carbonate minerals ($CdCO_3$) and complexation with functional groups (carboxyl and hydroxyl)	(Chen et al., 2019)
Pennisetum sp. straw biochar modified with $KMnO_4$ impregnation	90.3	300	Mainly due to precipitation (e.g., the binding of Cd and –OH), surface complexation, and the electrostatic interaction.	(Yin et al., 2019)
$KMnO_4$-treated magnetic biochar from rice husk	79.0	600	Oxygen functional groups and minerals	(Sun et al., 2019)
Birnessite-loaded rice husk biochar	9.1	600	Cd mainly occupied in vacant interlayer sites by forming complex with functional groups and O atoms in birnessite structure	(Wang et al., 2019)
Poultry litter biochar	52.1	500	Complexation and precipitation were the predominant adsorption mechanisms	This study
H_3PO_4/MgO-engineered biochar	113	500	Complexation and precipitation were the predominant adsorption mechanisms	This study

References

Agency for Toxic Substances & Disease Registry – ATSDR, 2017. Substance Priority List (https://www.atsdr.cdc.gov/SPL/).

Bayazit, S.S., Kerkez, O., 2014. Hexavalent chromium adsorption on superparamagnetic multi-wall carbon nanotubes and activated carbon composites. Chem. Eng. Res. Des. 92, 2725–2733.

Brunauer, S., Emmet, P.H., 1938. BET method. J. Am. Chem. Soc. 60, 309.

Barret, E.P., Joiyner, L.G., Halenda, P.P., 1953. BJH method. J. Am. Chem. Soc. 73, 373.

Bashir, S., Zhu, J., Fu, Q., Hu, H., 2018. Comparing the adsorption mechanism of Cd by rice straw pristine and KOH-modified biochar. Environ Sci Pollut Res. 25, 11875–11883.

Bekiaris, G., Peltre, C., Jensen, L.S., Bruun, S., 2016. Using FTIR photoacoustic spectroscopy for phosphorus speciation analysis of biochars. Spectrochim. Acta A. 168, 29−36.

Bogusz, A., Oleszczuk, P., Dobrowolski, R., 2015. Application of laboratory prepared and commercially available biochars to adsorption of cadmium, copper and zinc ions from water. Bioresour. Technol. 196, 540-549.

Cai, Y., Li, C., Wu, D., Wang, W., Tan, F., Wang, X., Wong, P.K., Qia, X., 2017. Highly active MgO nanoparticles for simultaneous bacterial inactivation and heavy metal removal from aqueous solution. Chem. Eng. J. 312, 158–166.

Carneiro, J.S.S., Lustosa Filho, J.F., Nardis, B.O., Ribeiro-Soares, J., Zinn, Y.L., Melo, L.C.A., 2018. Carbon stability of engineered biochar-based phosphate fertilizers. ACS Sustainable Chem. Eng. 11, 14203–14212.

Chen, S., Wang, J., Wu, Z., Deng, Q., Tu, W., Dai, G., Zheng, Z., Deng, S., 2018a. Enhanced Cr(VI) removal by polyethylenimine- and phosphorus-codoped hierarchical porous carbons. J. Colloid Interface Sci. 523, 110-120.

Chen, Z., Liu, T., Tang, J., Zheng, Z., Wang, H., Qi, S., Chen, G, Li, Z., Chen, Y., Zhu, J., Feng, T., 2018b. Characteristics and mechanisms of cadmium adsorption from aqueous solution using lotus seedpod-derived biochar at two pyrolytic temperatures. Environ. Sci. Pollut. Res. 25, 11854–11866.

Chen, Z., Zhang, J., Huang, L., Yuan, Z., Li, Z., Liu, M., 2019. Removal of Cd and Pb with biochar made from dairy manure at low temperature. J Integr Agr. 18, 201-210.

Cui, L., Chen, T., Yin, C., Yan, J., Ippolito, J.A., Hussain, Q., 2019. Mechanism of Adsorption of Cadmium and Lead Ions by Iron-activated Biochar. BioResources , 14, 842-857.

Demey, H., Vincent, T., Guibal, E., 2018. A novel algal-based sorbent for heavy metal removal. Chem. Eng. J. 332, 582-595.

Deng, Y., Huang, S., Laird, D.A., Wang, X., Dong, C., 2018. Quantitative mechanisms of cadmium adsorption on rice straw- and swine manure-derived biochars. Environ Sci Pollut Res. 25, 32418–32432.

Dalólio, F.S., Silva, J.N., Oliveira, A.C.C., Tinoco, I.F.F., Barbosa, R.C., Resende, M.O., Albino, F.L.T., Coelho, S.T., 2017. Poultry litter as biomass energy: A review and future perspectives. Renew Sust. Energ. Rev. 76, 941-949.

Foo, K.Y., Hameed, B.H., 2010. Insights into the modeling of adsorption isotherm systems Chem. Eng. J. 156 2-10.

Hass, A., Lima, I.M., 2018. Effect of feed source and pyrolysis conditions on properties and metal sorption by sugarcane biochar. Environ Technol. Innov.10, 16-26.

Hazra, B., Wood, D.A., Vishal, V., Varma, A.K., Sakha, D., Singh, A.K., 2018. Porosity controls and fractal disposition of organic-rich Permian shales using low-pressure adsorption techniques. Fuel. 220, 837-848.

Huang, F., Gao, L., Deng, J., Chen, S., Cai, K., 2018. Quantitative contribution of Cd2+ adsorption mechanisms by chicken-manure-derived biochars. Environ. Sci. Pollut. Res. 25, 28322–28334.

Idrees, M., Batool, S., Hussain, Q., Ullah, H., Al-Wabel, M.I, Ahmad, M., Kong, J., 2016. High-efficiency remediation of cadmium (Cd^{2+}) from aqueous solution using poultry manure–and farmyard manure–derived biochars. Sep. Sci. Technol. 51, 2307-2317.

Jazini, R., Soleimani, M., Mirghaffari, N., 2018. Characterization of barley straw biochar produced in various temperatures and its effect on lead and cadmium removal from aqueous solutions. Water Environ. J. 32, 125–133.

Kabata-Pendias, A., 2011. Trace Elements in Soils and Plants, 4 edition, CRC Press.

Karunanayake, A.G., Todd, O.A., Crowley, M., Ricchetti, L., Pittman Jr., C.U., Anderson, R., Mohan, D., Mlsna, T., 2018. Lead and cadmium remediation using magnetized and nonmagnetized biochar from Douglas fir. Chem. Eng. J. 331, 480-491.

Kousha, M., Daneshvar, E., Sohrabi, M.S., Jokar, M., Bhatnagar, A., 2012. Adsorption of acid orange II dye by raw and chemically modified brown macroalga Stoechospermum marginatum, Chem. Eng. J. 192, 67–76.

Freundlich, H. M. F., 1906. über die adsorption in lösungen. Zeitschrift für Physikalische Chemie, 57, 385–470.

Langmuir, 1916. The constitution and fundamental properties of solids and liquids. J. Am. Chem. Soc. 38, 2221–2295.

Lei, Shia, Y., Qiua, Y., Chec, L., Xue, C., 2019. Performance and mechanisms of emerging animal-derived biochars for immobilization of heavy metals. Sci Total Environ. 646, 1281-1289.

Lian, F., Xing, B., 2017. Black carbon (biochar) in water/soil environments: molecular structure, sorption, stability, and potential risk. Environ. Sci. Technol. 23, 13517–13532.

Liang, Y.,Cao, X., Zhao, L., Arellano, E., 2014. Biochar- and phosphate-induced immobilization of heavy metals in contaminated soil and water: implication on simultaneous remediation of contaminated soil and groundwater. Environ Sci Pollut R. 21, 4665–4674.

Liou, T., 2010. Development of mesoporous structure and high adsorption capacity of biomass-based activated carbon by phosphoric acid and zinc chloride activation. Chem. Eng. J. 158, 129–142.

Lustosa Filho, J.F., Penido, E.S., Castro, P.P., Silva, C.A., Melo, L.C.A., 2017. Co-Pyrolysis of Poultry Litter and Phosphate and Magnesium Generates Alternative Slow-Release Fertilizer Suitable for Tropical Soils. ACS Sustain. Chem. Eng. 10, 9043–9052.

Nist - Standard Reference Database, 2003. Version 3.4 (web version) (http:/srdata.nist.gov/xps/) .

Peng, H., Gao, P., Chu, G., Pan, B., Peng, J., Xing, B., 2017. Enhanced adsorption of Cu(II) and Cd(II) by phosphoric acid-modified biochars. Environ. Pollut. 229, 846-853.

Qambrani, N.A., Rahman, M.M., S Won, S Shim, Ra, C., 2017. Biochar properties and eco-friendly applications for climate change mitigation, waste management, and wastewater treatment: A review. Renew Sust. Energ. Rev. 79, 255–273.

Qi, F., Yan, Y., Lamb, D., Naidu, R., Bolan, N.S., Liu, Y., Ok, Y.S., Donne, S.W., Semple, K.T., 2017. Thermal stability of biochar and its effects on cadmium sorption capacity. Bioresour. Technol. 246, 48-56.

Shen, L., Zhang, L., Wang, K., Miao, L., Lan, Q., Jiang, K., Lu, H., Li, M., Li, Y., Shen, B., Zheng, W., 2018. Analysis of oxidation degree of graphite oxide and chemical structure of corresponding reduced graphite oxide by selecting different-sized original graphite. RSC Adv. 8, 17209-17217.

Shen, Y., Li, H., Zhu, W., Ho, S.H., Yuan, W., Chen, J., Xie, Y., 2017. Microalgal-biochar immobilized complex: A novel efficient biosorbent for cadmium removal from aqueous solution. Bioresour. Technol. 244, 1031-1038.

Silva, T.L., Cazetta, A.L., Souza, P.S.C., Zhang, T., Asefa, T., Almeida, V.C., 2018. Mesoporous activated carbon fibers synthesized from denim fabric waste: Efficient adsorbents for removal of textile dye from aqueous solutions. J. Clean. Prod. 171, 482-490.

Simonin, J., 2016. On the comparison of pseudo-first order and pseudo-second order rate laws in the modeling of adsorption kinetics. Chem Eng J. 15, 254-263.

Sips, R., 1948. On the Structure of a Catalyst Surface. J. Chem. Phys. 16.

Sun, C., Chen, T., Huang, Q., Wang, J., Lu, S., Yan, J., 2019. Enhanced adsorption for Pb(II) and Cd(II) of magnetic rice husk biochar by KMnO4 modification. Environ. Sci. Pollut. Res. 1-12.

Tan, X., Liu, Y., Gu, Y., Xu, Y., Zeng, G., Hu, X., Liu, S., Wang, X., Liu, S., Li, J., 2016. Biochar-based nano-composites for the decontamination of wastewater: A review. Bioresour Technol. 212, 318-333.

Tan, X., Liu, S., Liu, Y., Gu, Y., Zeng, G., Hu X., Wan, X., Liu, S., Jiang, L., 2017. Biochar as potential sustainable precursors for activated carbon production: Multiple applications in environmental protection and energy storage. Bioresour Technol. 227, 359-372.

Tian G, Wang W, Zong L, Wang A., 2017. MgO/palygorskite adsorbent derived from natural Mg-rich brine and palygorskite for high-efficient removal of Cd(II) and Zn(II) ions. J. Environ. Chem. Eng. 5, 1027–1036.

Thommes, M., Kaneko, K., Neimark, A.V., Olivier, J.P., Rodriguez-Reinoso, F., Rouquerol, J., Sing, K.S.W., 2015. Physisorption of gases, with special reference to the evaluation of surface area and pore size distribution (IUPAC Technical Report) Pure Appl. Chem. 87, 1051–1069.

USEPA - Toxicity characteristic leaching procedure, method 1311, 1992. Link: https://www.epa.gov/sites/production/files/2015-12/documents/1311.pdf.

Wang, B., Gao, B., Wan, Y., 2018. Entrapment of ball-milled biochar in Ca-alginate beads for the removal of aqueous Cd(II). J. Ind. Eng. Chem. 61, 161-168.

Wang, Y., Liu, R., 2018. H2O2 treatment enhanced the heavy metals removal by manure biochar in aqueous solutions. Sci Total Environ. 628-629, 1139-1148.

Wang, H., Chen, P., Zhu, Y., Cen, K., Sun, G., 2019. Simultaneous adsorption and immobilization of As and Cd by birnessite-loaded biochar in water and soil. Environ. Sci. Pollut. Res. 1 - 10

Wei, D., Ngo, H.H., Guo, W., Xu, W., Du, B., Khan, M.S., Wei, Q., 2018. Biosorption performance evaluation of heavy metal onto aerobic granular sludge-derived biochar in the presence of effluent organic matter via batch and fluorescence approaches. Bioresour. Technol. 249, 410-416.

Wei, S., Zhu, M., Fan, X., Song, J., Peng, P., Li, K., Jia, W., Song, H., 2019. Influence of pyrolysis temperature and feedstock on carbon fractions of biochar produced from pyrolysis of rice straw, pine wood, pig manure and sewage sludge, Chemosphere, 218, 624-631.

Xu, X.; Hu, X.; Ding, Z.; Chen, Y., 2017. Effects of copyrolysis of sludge with calcium carbonate and calcium hydrogen phosphate on chemical stability of carbon and release of toxic elements in the resultant biochars. Chemosphere, 189, 76−85.

Yin, G., Bi, L., Song, X., Luo, H., Ji, P., Lin, Q., Liu, Q., Tang, G., 2019. Adsorption of Cd(II) from aqueous solution by Pennisetum sp. straw biochars derived from different modification methods. Environ. Sci. Pollut. Res. 1-9.

Yu, W., Lian, F., Cui, G., Liu, Z., 2018. N-doping effectively enhances the adsorption capacity of biochar for heavy metal ions from aqueous solution. Chemosphere. 193, 8-16.

Zeng, Z., Tan, X., Liu, Y., Tian, S., Zeng, G., Jiang, L., Liu, S., Li, J., Liu, N., Yin, Z., 2018. Comprehensive Adsorption Studies of Doxycycline and Ciprofloxacin Antibiotics by Biochars Prepared at Different Temperatures. Front. Chem., 6, 1 - 11.

Zhao, L.; Cao, X.; Zheng, W.; Scott, J. W.; Sharma, B. K.; Chen, X., 2016. Copyrolysis of biomass with phosphate fertilizers to improve biochar carbon retention, slow nutrient release, and stabilize heavy metals in soil. ACS Sustainable Chem. Eng, 4, 1630−1636.

Zhao, L.; Zheng, W.; Mašek, O.; Chen, X.; Gu, B.; Sharma, B. K.; Cao, X., 2017. Roles of phosphoric acid in biochar formation: synchronously improving carbon retention and sorption capacity. J. Environ. Qual. 46, 393−401.

Zhou, Z., Xu, Z., Feng, Q., Yao, D., Yu, J., Wang, D., Lv, S., Liu, Y., Zhou, N., Zhong, M., 2018. Effect of pyrolysis condition on the adsorption mechanism of lead, cadmium and copper on tobacco stem biochar. J. Clean. Prod. 187, 996-1005.

Supplementary material

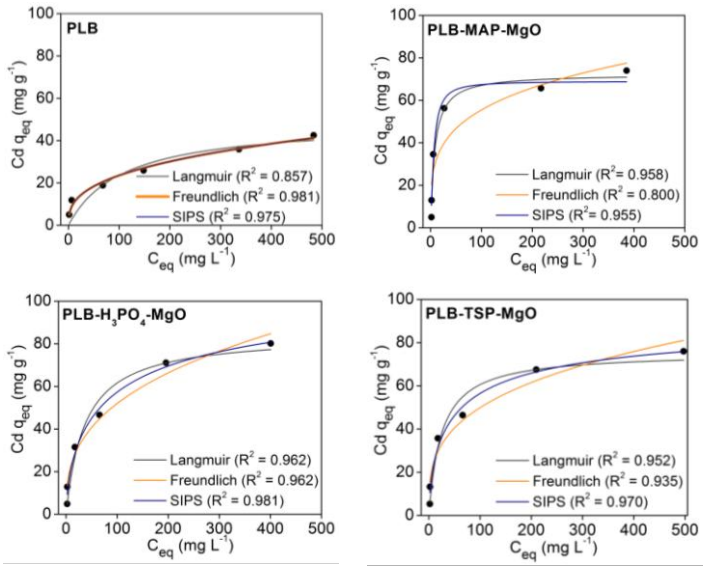

Figure A. Adsorption isotherms of biochars.

A) PLB

Carbon 1s Oxygen 1s Phosphorous 2p

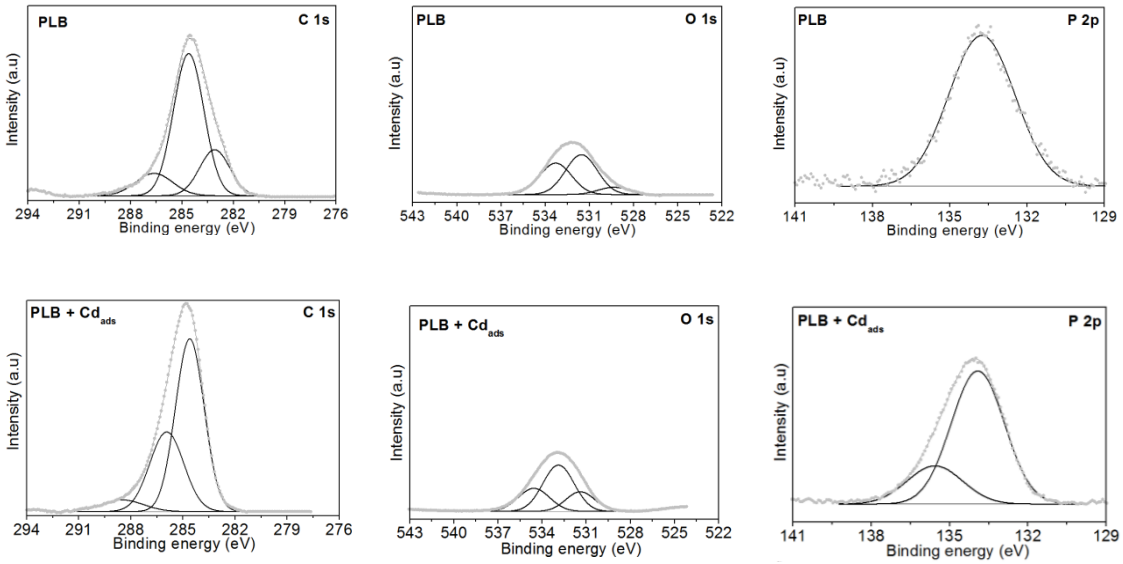

B) PLB-MAP-MgO

Carbon 1s Oxygen 1s Phosphorous 2p

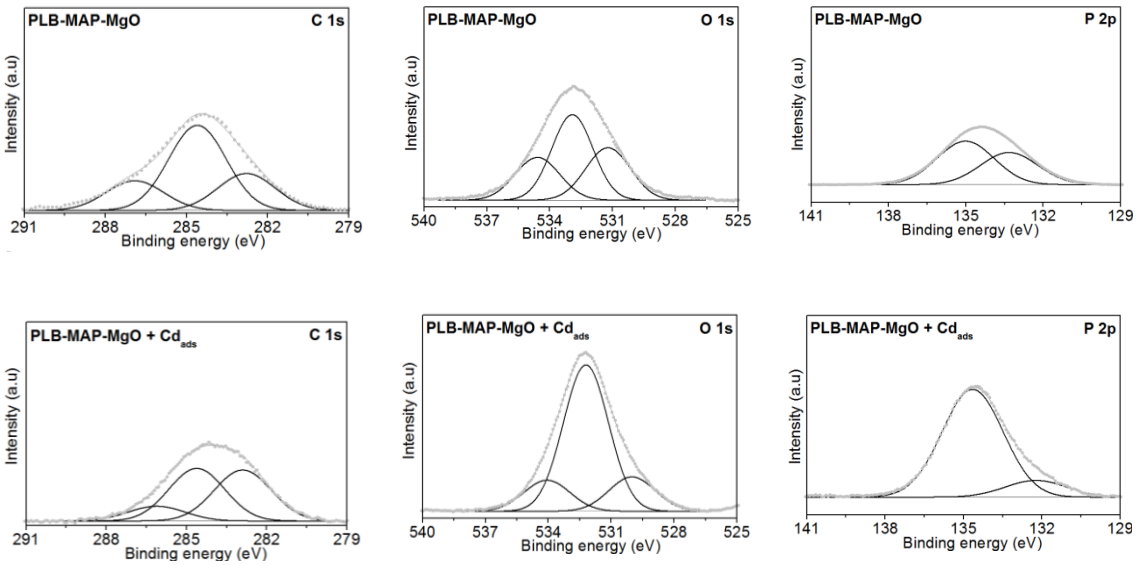

C) PLB-H_3PO_4-MgO

Carbon 1s Oxygen 1s Phosphorous 2p

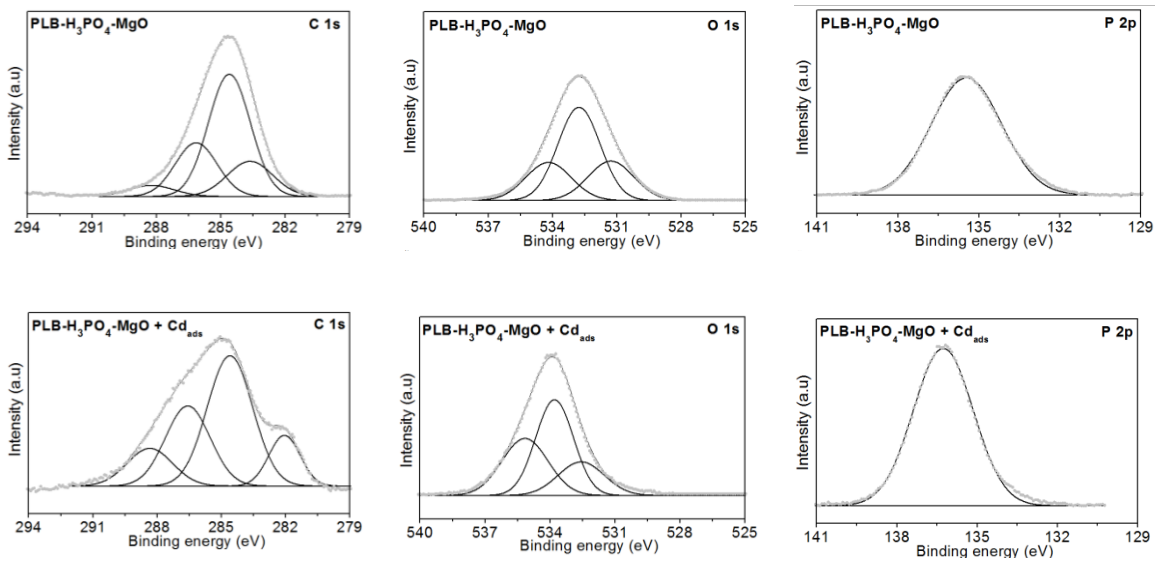

Figure B. Deconvolution of C1s, O1s, and P2p XPS spectra of biochars before and after adsorption.

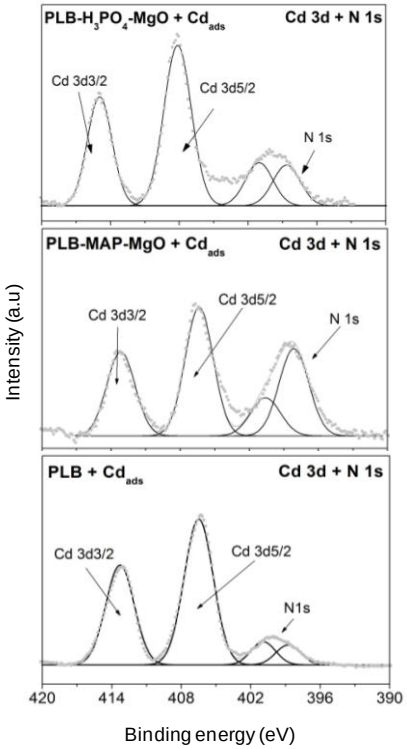

Figure C. Deconvolution of Cd 3d XPS spectra of biochars after adsorption.

MANUSCRIPT 2: SPECTROSCOPIC INVESTIGATION OF Pb^{2+} RETENTION ON PHOSPHORUS/MAGNESIUM-ENGINEERED BIOCHARS

Evanise Silva Penido[a], Maria Lucia Bianchi[a], Guilherme Lopes[b], Bárbara Olinda Nardis[b], José Ferreira Lustosa Filho[b], Luiz Roberto Guimarães Guilherme[b], Leônidas Carrijo Azevedo Melo[b*]

(Manuscript written according to the standards of NBR 6022 (ABNT, 2003))

[a]Federal University of Lavras, Chemistry Department, 3037, 37200-000, Lavras, Minas Gerais, Brazil.
[b]Federal University of Lavras, Soil Science Department, 3037, 37200000, Lavras, Minas Gerais, Brazil.

[*]Corresponding author:

Melo, L.C.A

Soil Science Department
Federal University of Lavras
Lavras, Minas Gerais, Brazil
e-mail: leonidas.melo@ufla.br

ABSTRACT

This study aimed to determine the efficiency of Pb^{2+} removal by phosphorus/magnesium-engineered biochars through batch assays and to elucidate the retention mechanisms, using advanced characterization methods. Biochars were produced from co-pyrolysis of poultry litter and monoammonium phosphate ($NH_4H_2PO_4$) or phosphoric acid (H_3PO_4) combined with magnesium oxide (MgO). Batch assays were carried out in aqueous medium and several characterization techniques were used to investigate the surface of biochars after Pb retention. The adsorption of Pb^{2+} ions on P/Mg-engineered biochars (up to 600 mg g^{-1}) was nearly 10 times more effective than on non-treated biochar (~60 mg g^{-1}). Fourier transform infrared spectroscopy studies showed that the functional groups on the surface of the biochars are modified during adsorption. Mapping obtained from scanning electron microscopy/energy dispersive X-ray spectroscopy showed that the contents of P, Mg, and O were closely related to adsorbed Pb. X-ray photoelectron spectroscopy showed changes in the surface chemical characteristics of the biochars before and after Pb^{2+} adsorption, proving that P and O groups interacted with Pb through chemisorption (precipitation and complexation). Insoluble lead apatites (PO_4^{3-}) where formed on the surface of the P/Mg-engineered biochars, as well as other Pb inorganic crystalline components, including hydrocerussite ($Pb_3(CO_3)_2(OH)_2$) and cerussite ($PbCO_3$), as revealed by the X-ray powder diffraction patterns and confirmed by X-ray absorption near edge structure. Thus, P/Mg-engineered biochars produced from poultry litter are considered effective and eco-friendly adsorbents for Pb-contaminated aqueous environments, such as wastewater.

Keywords: Co-pyrolysis. Synchrotron radiation. X-ray absorption. Adsorption mechanisms. Contamination

1 INTRODUCTION

Contamination of soil and water systems by potentially toxic elements is of great concern because of their toxicity and accumulation in the environment. Lead (Pb) exposure can pose serious threats to human health due to biological accumulation and high toxicity (KABATA-PENDIAS, 2011; PATRICK, 2006). Thus, it is of great importance to find appropriate treatments to alleviate toxic metal exposure and accumulation, especially considering low-cost and eco-friendly solutions.

Biochars, the solid products obtained from thermal treatment of any biomass in the absence or under low oxygen contents, have lately been widely investigated as promising biosorbents of toxic metals (ZHOU et al., 2018; ABDALLAH et al., 2019; LEE et al., 2019). The advantage of using biochars for immobilizing contaminants, over most conventional sorbents, is their suitable chemical and physical characteristics, such as porous structure, high surface area, and high functionality (QAMBRANI et al., 2017), as well as the possibility of reusing residues that are produced in large quantities and sometimes present difficulties of final disposal. For example, poultry litter is a residue generated in large quantities by the broiler meat sector, especially in Brazil, which is considered the second world broiler producer generating nearly 8–10 million tons per year (DALÓLIO et al., 2017).

Surface modifications of biochars have been applied for improving their physicochemical properties aiming to increase their removal capacity of both inorganic and organic contaminants from wastewater (WANG & WANG, 2019; PREMARATHNA et al., 2019). Recent studies have been focusing on the so-called engineered biochars, which can be prepared via impregnation of regular biochars with metal oxides, clay minerals, organic compounds, or other carbonaceous materials, which greatly alter their surface functionalities (AHMED et al., 2016; SIZMUR et al., 2017). For example, loading phosphate on biochars via co-pyrolysis can be considered a promising way to mitigate Pb pollution in wastewater (GAO et al., 2019). Besides increasing the biochar's affinity for toxic metals (CHEN et al., 2018; CHEN et al., 2019a), the impregnation of biomass with phosphate compounds prior to pyrolysis can increase the yield and the chemical, biological, and thermal stability of biochars, while reducing carbon losses during the heat treatment (XU et al., 2017; CARNEIRO et al., 2018). Magnesium oxide (MgO), a non-toxic and cost-efficient substance, is already considered a high-efficient adsorbent for a wide range of pollutants (CHOWDHURY et al., 2016; JIN et al., 2016). Lately, phosphorus/magnesium biochars have been prepared by our

research group and successfully tested as biochar-based fertilizers (LUSTOSA FILHO et al. 2017; LUSTOSA FILHO et al., 2019) and as adsorbents for Cd ions (PENIDO et al., 2019).

Since metal adsorption can occur in a variety of ways, such as (i) ion-exchange; (ii) metal-ligand complexation; (iii) cation-π bonding; and/or, (iv) surface (co)precipitation (LEI et al., 2019), it is essential to understand the binding mechanisms between metal ions and the engineered/functionalized biochars under environmentally-relevant aqueous conditions. X-ray absorption fine structure spectroscopy (XAFS), using synchrotron radiation, is a powerful tool to unravel the composition and bonding environments of the metallic elements and the biochar (XIONG et al., 2013; LI et al., 2019). For example, studies conducted by Wu et al. (2017), using XAS, revealed that the main Pb species observed in a nitrogen chemically-modified biochar after the adsorption process were $Pb(C_2H_3O_2)_2$, $PbSO_4$, Pb-Al_2O_3, and $Pb_3(PO_4)_2$, which favored the immobilization of Pb in aqueous solution. Furthermore, Fourier transform infrared spectroscopy (FTIR), X-ray diffraction (XRD), and X-ray photoelectron spectroscopy (XPS) as well as microscopic techniques such as scanning electron microscopy with energy dispersive X-ray spectrometry (SEM/EDX) are powerful complementary techniques that have been used to elucidate surface modifications and toxic metals retention mechanisms (LI et al., 2019; WU et al., 2017).

Therefore, in this study, advanced and complementary characterization methods (*e.g.*, FTIR, XPS, XRD, SEM/EDX, and XAFS) were used to investigate the adsorption of Pb^{2+} in aqueous solution by P/Mg-engineered biochars. The specific objectives of this work were: i) to determine the efficiency of Pb^{2+} removal through batch assays; and, ii) to elucidate the mechanisms of Pb^{2+} retention onto biochars, exploring features such as speciation and local coordination. With that, we ought to provide sufficient theoretical basis on the application of P/Mg-engineered biochars for environmental remediation concerning potentially toxic metals.

2 MATERIAL AND METHODS

2.1 Biochar preparation from poultry litter

Poultry litter (PL) samples used in this study were collected from a farm in the State of Minas Gerais, Brazil (21°13′34″ S and 44°58′31″ W) and next air-dried at room temperature as well as ground to pass through a 20-mesh sieve (<1.00 mm), prior to using. Separate aliquots of PL were mixed with monoammonium phosphate - MAP ($NH_4H_2PO_4$) and phosphoric acid (H_3PO_4) at a poultry litter/phosphate source ratio of 1:0.5 (w/w). To reduce

the residual acidity of the P compounds, magnesium oxide (MgO) was mixed at a P/Mg molar ratio of 1:1. The impregnated samples were pyrolysed at 500 °C for 2 h at a heating rate of 10 °C min^{-1}. Pyrolysis conditions were chosen aiming to maximize the yield and to increase carbon stabilization of the biochar (ZHAO et al., 2016; WEI et al., 2019), as well as to preserve the surface oxygen functional groups (CHEN et al., 2019b). The resulting biochars were identified as follows: PLB (poultry litter biochar), PLB-MAP-MgO, and PLB-H3PO4-MgO.

2.2 Batch adsorption and desorption experiments

A stock solution of Pb was prepared by dissolving $Pb(NO_3)_2$ in 0.01 mol L^{-1} $NaNO_3$ and dilutions were performed specifically to each batch assay. All experiments were performed in triplicate.

To assess the influence of pH on Pb^{2+} adsorption onto biochars, 0.1 mol L^{-1} NaOH or 0.1 mol L^{-1} HCl solutions were used to adjust the initial pH values of the Pb^{2+} solutions in the range of 2 to 9. A mass of 40 mg of each biochar was mixed with 10 mL of 300 mg L^{-1} Pb^{2+} for each pH value, followed by 24 h of stirring and membrane filtration (0.45-μm Millipore pore size). Next, pH at equilibrium was measured.

Batch kinetic experiments were performed using 40 mg of each biochar mixed with 10 mL of 300 mg L^{-1} of Pb^{2+} at pH 6.2 and agitated at room temperature (25 ± 1 °C) for predetermined time intervals of 5, 10, 15, 30, 60, 300, 720, and 1440 min, followed by membrane filtration (0.45-μm Millipore pore size).

Equilibrium isotherms were evaluated using 4.0 g L^{-1} of each biochar mixed with varying initial Pb^{2+} concentrations, which ranged from 20 to 600 mg L^{-1} for PLB and from 300 to 2500 mg L^{-1} for PLB-MAP-MgO and PLB-H3PO4-MgO, since the engineered biochars presented higher Pb^{2+} retention capacities. Metal concentrations in extracts were quantified by atomic absorption spectroscopy with air-acetylene flame (FAAS), using a Perkin Elmer Analyst 800 equipment.

Desorption tests were performed with biochars previously used in adsorption tests, as described previously. For that, samples retained in membrane filters were oven dried at 60 °C for 24 hours and next reacted with three different desorption solutions: i) 0.01 mol L^{-1} $CaCl_2$, which desorbs easily available fractions; ii) 1 mol L^{-1} HCl, which is a strong acid able to remove most Pb from solution; and iii) 0.1 mol L^{-1} acetic acid solution, according to the TCLP method (UNITED STATES ENVIRONMENTAL PROTECTION AGENCY, 1992),

which determines the mobility of an analyte in solid wastes. Desorption experiments were carried out using 0.1 g of Pb-loaded biochar in 10 mL of each solution, with 24 hours of stirring. The extracts were analyzed by inductively coupled plasma atomic emission spectroscopy (ICP-OES) for Pb.

In order to study the surface of the biochars after Pb retention using the characterization techniques described next, higher amounts of each biochar were used to adsorb Pb from aqueous solutions at the highest adsorption capacity obtained from the previous results of the adsorption isotherms.

2.3 Characterization techniques

Scanning electron microscopy with energy dispersive X-ray spectroscopy (SEM/EDX) (Carl Zeiss mod. EVO 50/ IXRF Systems mod. 500 Digital Processing) was used to characterize the chemical composition of the materials before and after Pb^{2+} adsorption. Fourier-transform infrared spectroscopy (FTIR) (Varian/mod. 660 IR) was used to identify the functional groups on biochars surface before and after Pb^{2+} adsorption. The spectra were investigated in the 4000-400 cm^{-1} region under a 4 cm^{-1} resolution, with 16 scans. X-ray photoelectron spectroscopy (XPS) (UNI-SPECS UHV) was performed to analyze the composition and chemical state of the surface elements of the materials using a k alpha Mg source, h_v 1253.6 eV before and after Pb^{2+} adsorption. The Pb-loaded biochars were analyzed using X-ray diffraction (XRD) to confirm the contribution of chemical precipitation for Pb removal. XRD analysis was carried out using a CuKα (0.154 nm) radiation, operated at 30 kV and 15 mA, with Ni filter for Kβ suppression, and detection with a scintillator of NaI and Be window. Peak identification was carried out based on mineralogy databases and related literature.

Pb-loaded biochar and standard samples were analyzed by X-ray absorption near edge structure (XANES) and extended X-ray absorption fine structure (EXAFS) at the Brazilian Synchrotron Light Laboratory (LNLS) on the XAFS2 beam line. The energy calibration was carried out using a Pb foil and was collected simultaneously with the spectrum of each sample. Powder samples were pressed into pellets to optimize the absorption step and total absorption. The transmission was measured at room temperature at the Pb-L_{III} edge (13,035 eV) with at least seven replications in order to obtain good signal-to-noise ratio. Data was processed using the Athena software. After normalization and background correction, the χ(k) function was used to isolate the scattering portion of the spectra. In order to identify and

quantify the Pb species prevailing in the biochar samples, linear combination fitting (LCF) was performed, using the EXAFS function (k^2 weighted), with k values ranging from 1 to 8 $Å^{-1}$.

3 RESULTS AND DISCUSSION

The basic properties of biochars can be found in our previous studies (PENIDO et al., 2019; LUSTOSA FILHO et al., 2017). Briefly, the pH values of PLB, PLB-MAP-MgO, and PLB-H3PO4-MgO were 11.1, 6.9, and 9.1, respectively, and the pH values at the point of zero charge of the biochars are 7.0, 6.1, and 5.5, respectively. The BET specific surface areas of biochars are considered low, i.e., PLB = 6.08 $m^2 g^{-1}$, PLB-MAP-MgO = 23.49 $m^2 g^{-1}$, and PLB-H3PO4-MgO = 5.81 $m^2 g^{-1}$. Penido et al. (2019) demonstrated that surface area was not the main control of Cd^{2+} adsorption. Instead, other reasons such as the reactivity of surface functional groups might have contributed more to Cd^{2+} retention, which can also be extended for Pb^{2+} in the present study.

3.1 Batch assays: Pb^{2+} removal from aqueous medium

The influence of pH on Pb^{2+} adsorption by biochars was measured over a pH range of 2.0 to 9.0 (Figure 1A). The lowest adsorption of Pb, especially for PLB, occurred at pH 2.0, and might be attributed to the competition between H^+ and Pb^{2+} for adsorption sites. Pb^{2+} adsorption was nearly unchanged for pH > 3 (Figure 1A), regardless of the initial pH adjustment. Ling et al. (2017) observed a similar effect, attributing this to the large number of functional groups, including OH, NH_2, C═O, COOH, and MgO, on the surface of MgO@N-biochar from plant material, which act as buffer agents to maintain pH in a relatively stable region. Furthermore, Wang et al. (2018) attributed little effects of pH changes on Pb^{2+} removal due to the dominance of the precipitation mechanism, which might explain that even at initial low pH values (pH = 2), the engineered biochars presented good retention capacities when compared with the other initial pH values and also with non-treated biochar (PLB). Moreover, the release of H_3O^+ from oxygen-containing functional groups after ion exchange with Pb^{2+} could also be responsible for the decrease in solution pH. Adsorption mechanisms underlying this reasoning will be further discussed. The equilibrium pH values of the biochars were nearly constant, around 5 and 6 (Figure 1A).

Retention of Pb^{2+} ions by the P/Mg-engineered biochars (PLB-MAP-MgO and PLB-H3PO4-MgO) was more effective than PLB, with a higher amount being adsorbed in a shorter equilibrium time (Figure 1B). P/Mg-engineered biochars reached equilibrium within only 30 minutes of contact, which is a desired property of adsorbents, while for PLB, equilibrium was reached only after 5 h. Typical kinetic models (pseudo-first-order and pseudo-second-order kinetic models) were used to describe the kinetic patterns. The pseudo-second-order kinetic model showed slightly higher R^2 values (Figure A, supplementary material in Appendix A), indicating that the reaction rate of Pb^{2+} adsorption depended more on the number of active sites and the rate-limiting step may be chemical adsorption, where covalent bonds and ionic bonds between Pb^{2+} and biochars play the main role (PREMARATHNA et al., 2019).

Figure 1 - Effect of pH on Pb^{2+} retention (mg g^{-1}) by biochars and solution equilibrium pH after 24 h of stirring (A); Effect of contact time on Pb^{2+} retention onto biochars (B); Pb^{2+} adsorption isotherms; and Pb^{2+} desorption (%) using different extractants (0.01 mol L^{-1} $CaCl_2$, 0.1 mol L^{-1} acetic acid (TCLP) and 1 mol L^{-1} HCl; 0.1 g of Pb-loaded biochar and 10 mL of solution (D).

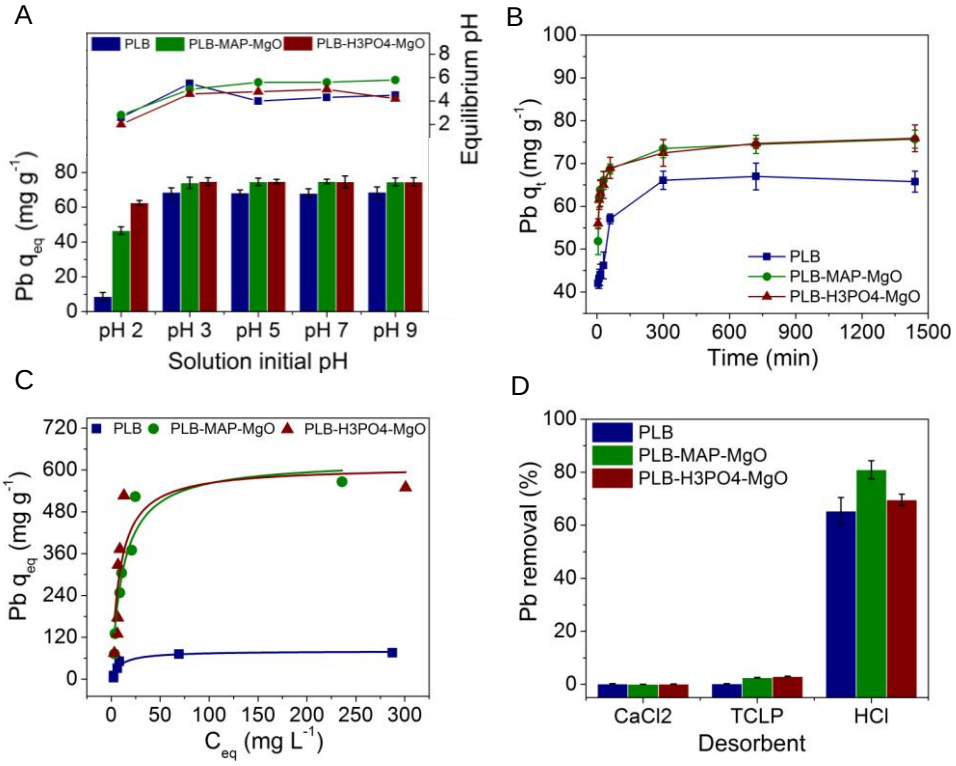

Source: from author (2019).

The maximum Pb^{2+} adsorption capacity increased significantly by approximately 10 times from 60 mg g^{-1} by PLB to up to 600 mg g^{-1} for PLB-MAP-MgO and PLB-H3PO4-MgO (Figure 1C).

The contents of Pb^{2+} desorbed from biochars in different extractants are shown in Figure 1D. Extraction using 0.01 mol L^{-1} $CaCl_2$ desorbed only up to 0.2% of Pb^{2+} from solution. As for TCLP, the maximum desorption capacities were in the range of 3% for PLB-MAP-MgO and PLB-H3PO4-MgO and only 0.2% for PLB, which shows the low leaching potential of these materials. Even when using 1.0 mol L^{-1} HCl, which is considered a strong acid, not all Pb was removed from biochars, proving once more that chemical adsorption plays an important role in the system. The maximum desorption percentage was found for PLB-MAP-MgO (80%).

The Pb^{2+} adsorption capacities of biochars were further compared with those of recently reported biochar-based adsorbents (Table 1).

Table 1. Comparison of maximum Pb^{2+} adsorption capacities by biochars with previously recent reported data.

Biochar	**Pb^{2+} maximum adsorption (mg g^{-1})**	**T (°C)**	**Reference**
Rice straw biochar	164.6	500	Shen et al. (2019)
Douglas fir biochar (magnetic)	40.0	900	Karunanayake et al. (2018)
Biochar-supported graphene oxide	26.1	600	Zhang et al. (2018)
Tobacco stem biochar	317	500	Zhou et al. (2018)
Pine wood/chitosan biochar	134.0	425	Dewage et al. (2018)
Ginkgo leaf biochar	138.9	800	Lee et al. (2019)
KOH-activated sludge-based biochar	57.5	700	Zhang et al. (2019)
Si-rich coconut fiber biochar	89.7	500	Li et al. (2019)
Eggshell-biochar composites	261.1	450	Wang et al. (2018)
Corn stover biochar	25.0	600	Mireles et al. (2019)
P-enriched biochar	4.84	600	Chen et al. (2019b)
Empty fruit bunch biochar	103.1	250	Fahmi et al. (2018)
Iron activated reed biochar	17.5	450	Cui et al. (2019)
Carbonized mushroom biochar	547.5	500	Abdallah et al. (2019)
Fe-Mn-S/biochar	182.0	800	Yang et al. (2019)
Rape straw + $Ca(H_2PO_4)_2$ biochar	117.3	500	Gal et al. (2019)
Rape straw + KH_2PO_4 biochar	323.0	500	Gal et al. (2019)
Poultry litter biochar (PLB)	72.0	500	This study
PLB-MAP-MgO	520.0	500	This study
PLB-H3PO4-MgO	522.0	500	This study

Compared with other adsorbents, the P/Mg-engineered biochars exhibited superior Pb^{2+} adsorption capacities in the majority of the cases. Similar values were found only by Abdallah et al. (2019) for carbonized mushroom biochar produced at 500 °C (up to 548 mg g^{-1}). Therefore, P/Mg-engineered biochar is a very promising Pb^{2+} adsorbent, produced from low-cost materials, with value-added utilization of the waste produced in large amounts by the broiler sector.

3.2 Biochar characterization: FTIR

The FTIR spectra of the biochars are shown in Figure 2. The bands around 1600 and 800 cm^{-1}, which represent aromatic carbon, are typically found for biochars (SHEN et al., 2019). The bands at around 1050 cm^{-1} are attributed to the stretching of C-O-C bonds. Both CH_2 and CH_3 appear at around 1450 - 1375 cm^{-1}, with more intensity for PLB. Non-treated biochar (PLB) presents more aromatic surface groups that are electron-rich π-systems that may donate π-electrons in acid-basic Lewis reactions (PENG et al., 2017), significantly contributing to Pb^{2+} adsorption, since bands decreased their intensities. C=C and C=O stretching can be found between 1680 - 1630 cm^{-1}. Asymmetrical stretch of P-O-P can be also assigned to bands at 945-925 cm^{-1}, which present more intensity for the P/Mg-engineered biochars when compared with PLB, showing the high abundance of P in the samples. Inorganic PO_4^{3-} can be found either around 1100-1000 cm^{-1} or 580-540 cm^{-1} and P=O at around 1350 cm^{-1} (SILVERSTEIN et al., 2014; CHEN et al., 2019a).

FTIR studies showed that the functional groups on the surface of the biochars are modified during adsorption. For example, bands related to phosphorus, below 1000 cm^{-1}, decreased in intensity, indicating interaction with Pb ions. Bands corresponding to C-O-C stretching vibration weakened and slightly shifted to lower wavenumbers, because most of the binding sites were used by metal ions for coordination, indicating that carbonyl groups participated in the adsorption process (ABDALLAH et al., 2019). There was a great decrease in the intensity of CO_3^{2-} band at 1480 cm^{-1} after Pb adsorption for sample PLB (Figure 2).

When Pb bonds to O-containing groups, it leads to a decrease in the electron cloud density of the oxygen atom, which reduces the binding energy of the groups, increasing their stability (KARUNANAYAKE et al., 2018).

Figure 2. FTIR spectra of biochars before and after Pb^{2+} adsorption.

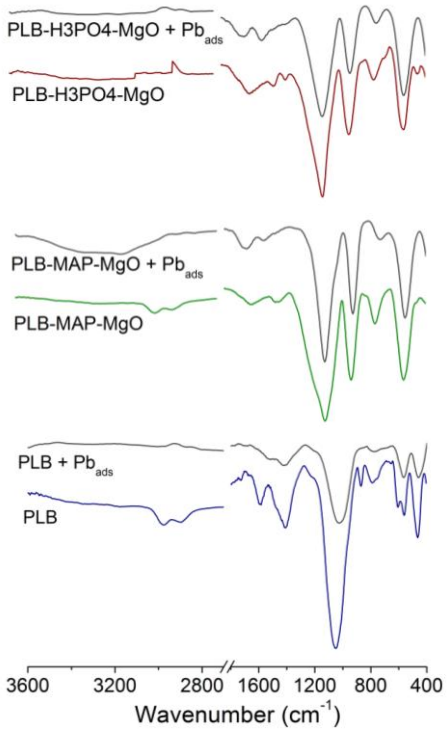

Source: from author (2019).

3.3 Biochar characterization: SEM/EDX

SEM/EDX mapping of biochars was analyzed to explore the surface functionalization with P and Mg as well Pb^{2+} adsorption (Figure 3). The contents of P and Mg increased dramatically after modification, revealing that the elements are successfully loaded on the surface of the biochars after co-pyrolysis, since biochars were washed with distilled water prior to analysis. The distribution of Mg and P was homogeneous throughout the surface of the P/Mg-engineered biochars (Figure 3B and C), with high correlation between adsorbed Pb and P and O, indicating that Pb adsorption might occur predominantly to phosphate and oxygen functional groups. As for PLB (Figure 3A), Pb distribution was more related to O than P. Calcium (Ca), silicon (Si) and potassium (K) (data not shown) were also detected by SEM/EDX in smaller quantities and are present on the surface of the biochars, especially for PLB-MAP-MgO.

Figure 3. SEM/EDX elemental maps of biochars.

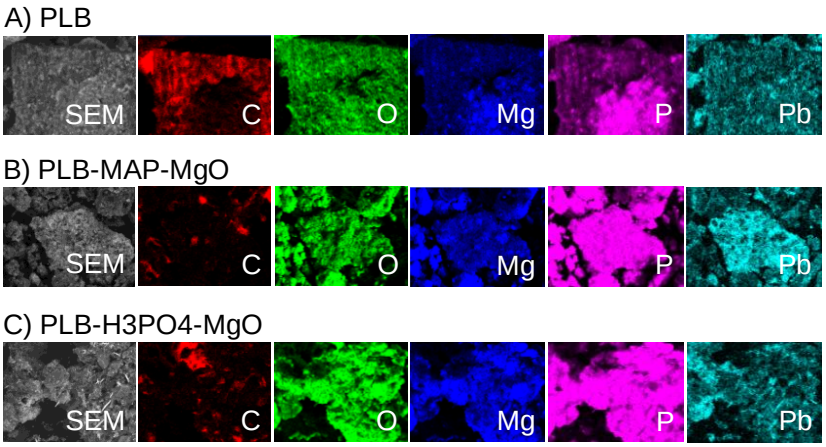

Source: from author (2019).

3.4 Biochar characterization: XPS

Deconvoluted XPS spectra analyses of biochars are shown in Fig. 4. XPS was used to analyze the changes in the surface chemical characteristics of the biochars before and after Pb^{2+} adsorption. This technique is appropriate for probing at the surface (up to 20 nm), where most of the adsorption reactions are expected to take place.

For C1s, the peak centered at 285.0 eV was assigned for C-C bonds, at 286.5 eV to C-OH bonds, and at 283.0 eV to C=O. Three peaks in the XPS spectrum of O1s can be associated with O-C=O, C-O and C=O at around 534.0, 532.0 and 529.0 eV.

The spectra for P2p show a signal at 133.2 eV in PLB (Figure 4C), two signals at 135 and 133 eV for PLB-MAP-MgO and one band at 135.5 eV for PLB-H3PO4-MgO, indicating that the P speciation of engineered biochars were different. Signals around 133 eV represents PO_4^{3-} and signals around 135 eV can correspond to P_2O_5. There was no difference between spectra before and after Pb^{2+} retention for PLB in the P2p chemical environment (Figure 4C), indicating low interaction with Pb. As for PLB-MAP-MgO, the peak at 135 eV increased its intensity, while the signal of PO_4^{3-} had its intensity decreased (Figure 4F). For PLB-H3PO4-MgO, besides presenting increased intensity, the peak shifted to higher binding energy after Pb^{2+} adsorption (Figure 4I). This result showed that the P groups interacted with Pb and promoted Pb removal, which resulted in an increase of outer electron cloud density in P atom (GAO et al., 2019).

Figure 4. XPS deconvoluted spectra of biochars before and after Pb^{2+} adsorption.

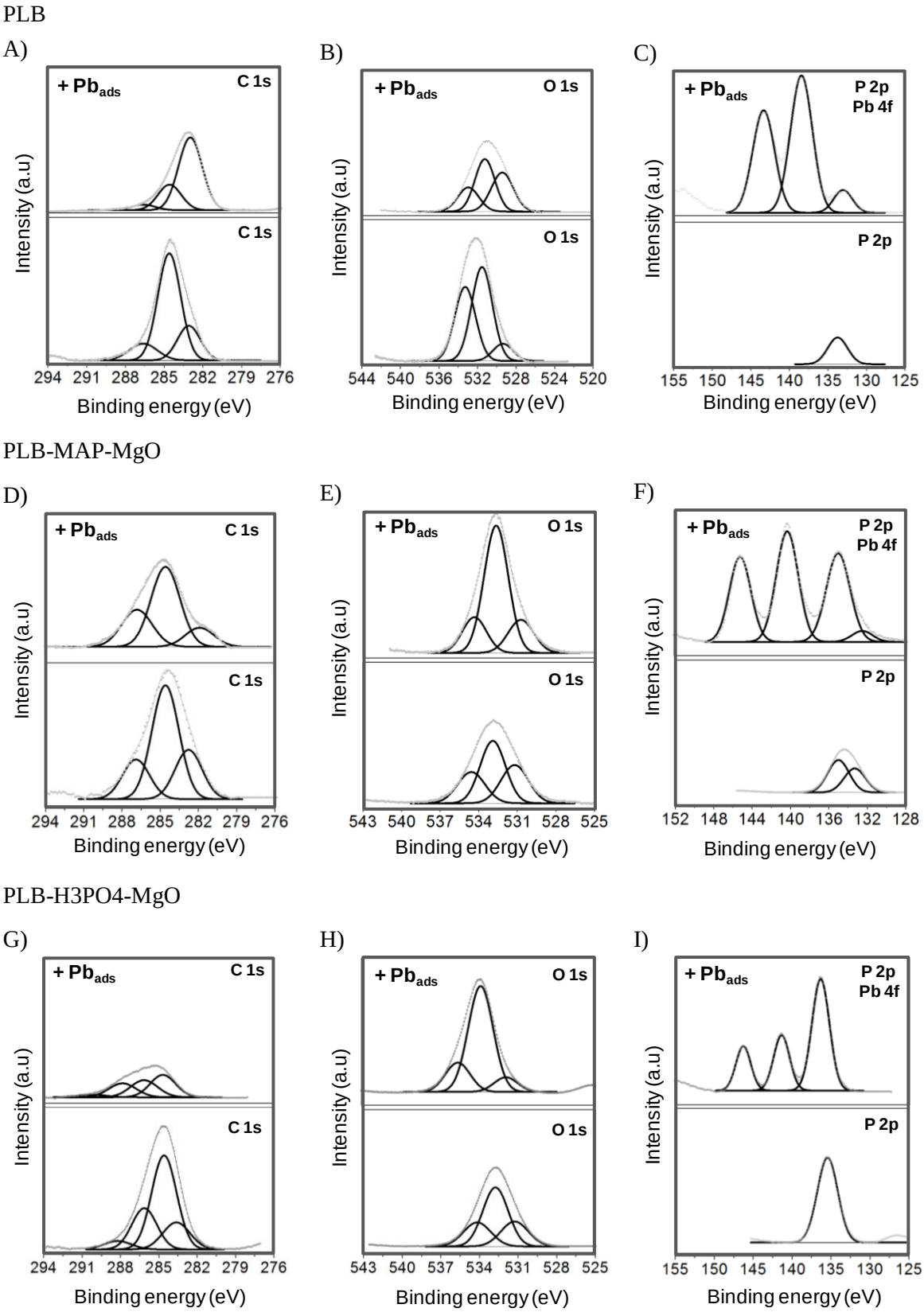

Source: from author (2019).

Two contributions, Pb $4f_{7/2}$ and Pb $4f_{5/2}$ resulting from the spin-orbit splitting was observed in all spectra of Pb-loaded biochars, indicating Pb^{2+} was successfully adsorbed on the biochar surface (Figure 4C, F and I). However, the binding energies are different for each biochar, which indicates that the chemical environments of Pb atom in the three biochars were different.

3.5 Biochar characterization: XRD

Several diffraction peaks related to Pb appeared in the XRD patterns of Pb-loaded biochars (Figure 5). Treatment with phosphate compounds and MgO, which increased the pH of the biochars, caused the formation of insoluble lead apatites on the surface of the P/Mg-engineered biochars, as observed in the XRD patterns. The positions of the lead apatite peaks varied slightly, which was consistent with the presence of lead apatites of different formulae: $Pb_{10}(PO_4)_6(OH)_2$, $Ca_2Pb_3(PO_4)_3Cl$, and $Pb_5(PO_4)_3Cl$. Dissolution from Mg-P association could have provided more P for Pb precipitation in samples PLB-MAP-MgO and PLB-H3PO4-MgO since these samples, which were characterized in our previous study (LUSTOSA FILHO et al., 2017), contain magnesium pyrophosphate ($Mg_2P_2O_7$) and magniotriplite $(Mg,Fe^{2+},Mn^{2+})_2(PO_4)(F,OH)$ in their structure.

Figure 5. Powder X-ray diffraction patterns (baseline-corrected) of Pb-loaded biochars showing Pb compounds. ♥ Hydropyromorphite ($Pb_{10}(PO_4)_6(OH)_2$); ★ Phosphohedyphane ($Ca_2Pb_3(PO_4)_3Cl$); ● Hydrocerussite ($Pb_3(CO_3)_2(OH)_2$); and ♦ Pyromorphite ($Pb_5(PO_4)_3Cl$). The prominent lead apatite peaks are shaded.

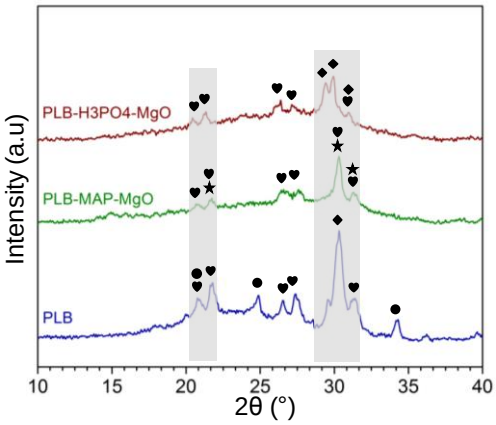

Source: from author (2019).

As for non-treated PLB, besides lead apatites, it also presented hydrocerussite ($Pb_3(CO_3)_2(OH)_2$). This result is in accordance with FTIR results previously described. Cao et al. (2009) found lead phosphate (β-$Pb_9(PO_4)_6$) and hydrocerussite ($Pb_3(CO_3)_2(OH)_2$) in Pb-loaded dairy-manure derived biochar.

3.6 Biochar characterization: XAS

XANES spectra of all Pb-loaded biochars and standard materials were very similar to that of the Pb^{2+} reference compounds regarding oxidation state (Figure 6A).

Figure 6. Lead L_{III}-edge near edge structure (XANES) spectra and k^2-weighted Fourier transforms of extended X-ray absorption fine structure (EXAFS) spectra of Pb-loaded biochars and the reference compounds (A); best linear combination fitting (LCF) results of samples against reference spectra, showing quantitative (%) Pb speciation for PLB (B), PLB-MAP-MgO (C) and PLB-H3PO4MgO (D). χ^2 and R-factor values indicate goodness of fit.

A)

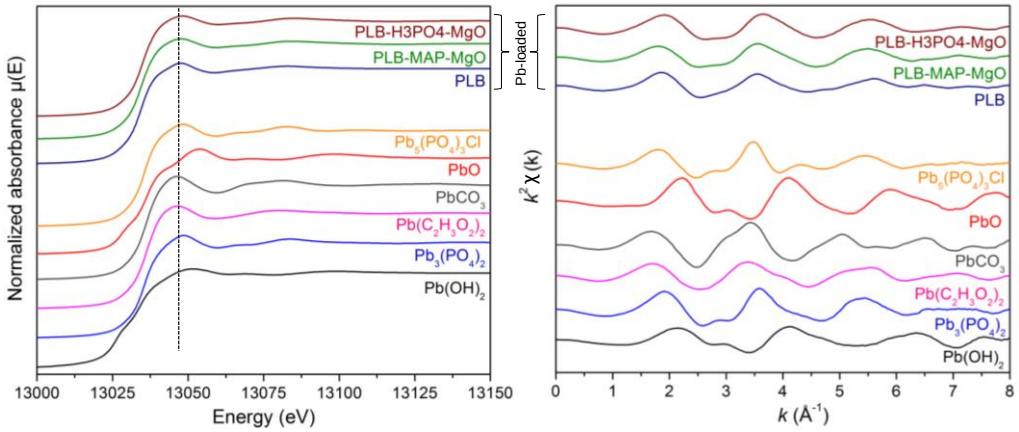

B) C) D)

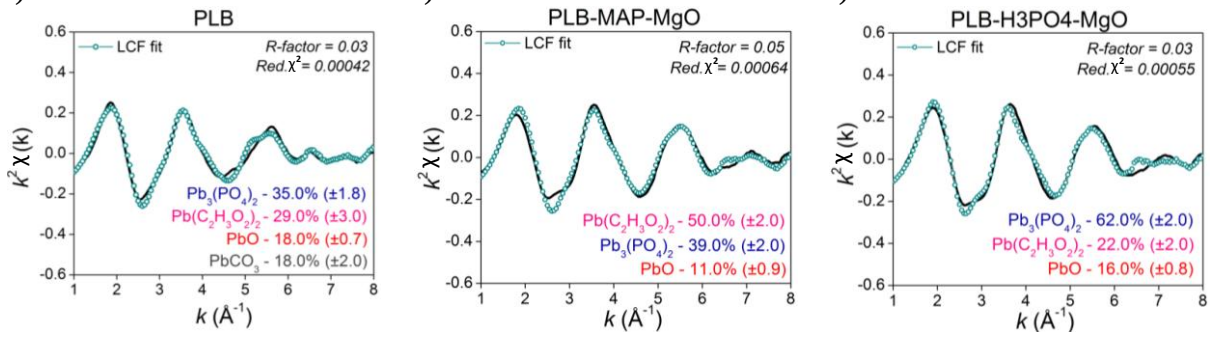

Source: from author (2019).

Linear combination fitting (LCF) results of the k^2-weighted EXAFS spectra are shown in Figure 6 (B, C and D), in which the low values of χ^2 and R-factor indicate goodness of fit.

The results showed that $Pb_3(PO_4)_2$, $Pb(C_2H_3O_2)_2$, and PbO were the three most important Pb species present on Pb-loaded biochars. Non-treated biochar (PLB) also presented 18% of $PbCO_3$, which is in accordance with the XRD results, in which the pattern for the mineral hydrocerussite ($Pb_3(CO_3)_2(OH)_2$) was found. Sample PLB-H3PO4-MgO presented the highest percentage of $Pb_3(PO_4)_2$ (62%), followed by PLB-MAP-MgO (39%) and PLB (35%). The percent of Pb associated with O-containing groups were higher for PLB.

Sanderson et al. (2015) showed that Pb precipitated as PbO with MgO, which was present in the form of periclase (cubic form of MgO) and magnesium hydroxide ($Mg(OH)_2$). Thus, treatment with MgO in the present study could have had similar effect, considering the formation of PbO.

Wu et al. (2017) found that the five most predominant Pb species in Pb-loaded biochar chemically modified with ammonia and nitric acid were $Pb(C_2H_3O_2)_2$, $Pb_3(PO_4)_2$, Pb-loaded montmorillonite, $PbSO_4$ and Pb-Al_2O_3.

Further studies on the specific molecular or atomic combination, valence bond and bond length of the adsorbed forms of Pb onto the biochar surfaces should be performed by EXAFS analysis, for a better understanding about the binding stability.

3.7 Overall mechanism

Since lead is known to be present mainly as Pb^{2+} at pH near 5.5 in natural aquatic system (UCUN et al., 2003), those Pb species interacted with the surface groups present on the biochars, especially O and P-containing groups. Complexation and precipitation were found to be the predominant mechanisms.

As for complexation, FTIR showed chelation of Pb with carboxyl groups on the biochar. Electrostatic interactions and ion exchanges could also be slightly responsible for Pb removal, especially considering the amounts of Mg present in the engineered biochars. However, the contribution of physisorption is minor considering that the desorption studies showed that Pb is not easily extracted from the surface of the materials. Nevertheless, when Mg is released to solution, Pb ions could replace it to form C−O−Pb−O−C, which are considered very stable structures (LI et al., 2019). Li et al. (2018) also revealed that Pb was readily chelated by two −COOH groups to form the structure of $(-O-C=O)_2Pb$ during Pb adsorption to MgO hybrid sponge-like carbonaceous material. Pb−O−P chains also occurred in the atomic environment around Pb in Pb-loaded biochars, as demonstrated by XPS analysis.

Figure 7. Illustration of the mechanisms of Pb^{2+} retention, showing coordination and precipitation.

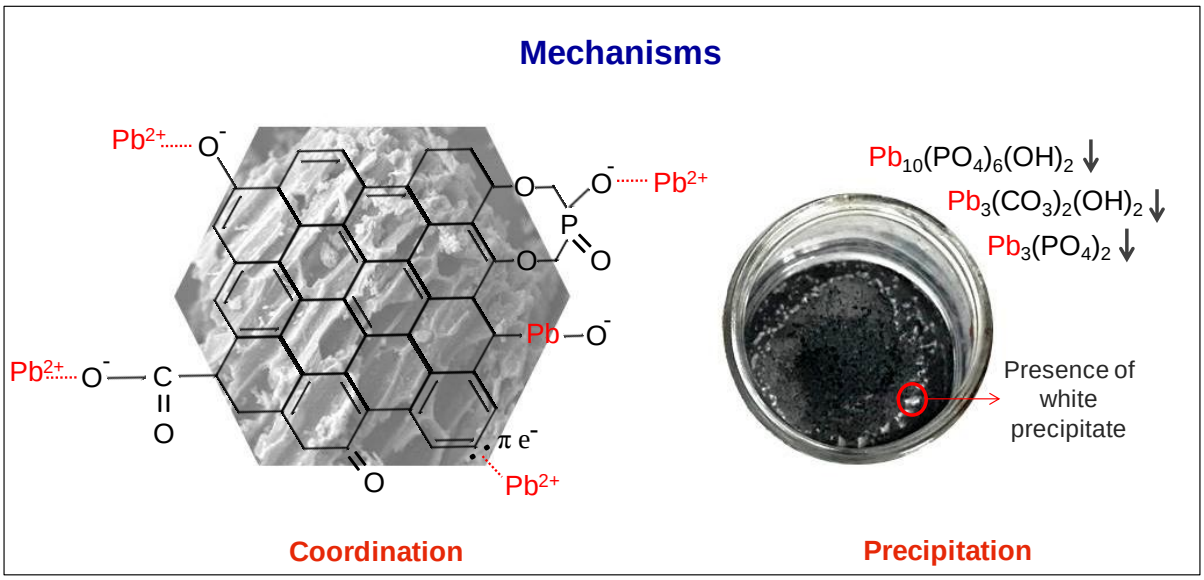

Source: from author (2019).

Indeed, in the study, spectroscopy techniques showed that the active sites of the organic skeleton of the biochars, presenting carboxyl functional groups, played a significant role on the adsorption mechanism.

Precipitation as lead apatites played an important role in the retention of Pb on the surface of the biochars as well, which also explains the highly effective adsorption capacities of the P/Mg-engineered biochars that provide more phosphorus to form precipitation with Pb. Since $Pb_5(PO_4)_3Cl$ presents very low solubility, more stable pyromorphite are formed by these biochars. Furthermore, in a aqueous medium presenting OH^-, Pb ions can precipitate according to the following equation: $2HCO_3^- + 3Pb^{2+} + 4OH^- \rightarrow Pb_3(CO_3)_2(OH)_2 + 2H_2O$ (CAO et al., 2009).

Figure 7 shows a schematic illustration of the mechanism of retention, showing coordination of Pb d-electron to C=C (π-electrons) bonds, O-containing groups and phosphate groups as well as precipitate formation.

4 CONCLUSION

The results showed that the impregnation of P and Mg in the production of poultry litter biochars was effective in functionalizing the surface of the materials and to increase the aromaticity of the biochars. Phosphorus played an important role to Pb^{2+} removal in solution

by the P/Mg-engineered biochars, which presented much higher Pb^{2+} removal capacity than the original biochar, especially due to precipitation as lead apatites. $Pb_3(PO_4)_2$, $Pb(C_2H_3O_2)_2$, and PbO were the three most important Pb species present on Pb-loaded biochars. Moreover, spectroscopy studies showed that coordination and precipitation were the most important retention mechanisms.

The conversion of renewable biomass from chicken residues into functional P/Mg-engineered biochars to be used as adsorbents is beneficial not only for waste management purposes, considering that the residue is produced in large scale, but also for wastewater treatment, due a highly-efficient retention capacity of the engineered biochars. The present study provides a basis for a successful practical application of the biochars in environmental remediation. Future studies can focus on heavy-metal polluted soils using the p/Mg-engineered biochars as amendments under either controlled or field conditions.

Acknowledgements

The authors would like to thank the Minas Gerais State Agency for Research and Development – FAPEMIG for financial support and scholarship to the first author. This study was financed in part by the Coordenação de Aperfeiçoamento de Pessoal de Nível Superior – Brasil (CAPES) – Finance Code 001. The National Council for Scientific and Technological Development (CNPq) are also acknowledged.

REFERENCES

ABDALLAH, M. M.; AHMAD, M. N.; WALKERT, G.; LEAHY, J. J.; KWAPINSKI, W. Batch and Continuous Systems for Zn, Cu, and Pb Metal Ions Adsorption on Spent Mushroom Compost Biochar. **Industrial & Engineering Chemistry Research**, v. 58, p. 7296–7307, 2019.

AHMED, M.B.; ZHOU, J. L.; NGO, H. H.; GUO, W.; CHEN, M. Progress in the preparation and application of modified biochar for improved contaminant removal from water and wastewater. **Bioresource Technology**, v. 214, p. 836-851, 2016.

ASSOCIAÇÃO BRASILEIRA DE NORMAS TÉCNICAS. **NBR 6022**: Informação e documentação: artigo em publicação periódica científica impressa. Rio de Janeiro, 2003.

CARNEIRO, J. S. S.; LUSTOSA FILHO, J. F.; NARDIS, B. O.; RIBEIRO-SOARES, J.; ZINN, Y. L.; MELO, L. C. A. Carbon stability of engineered biochar-based phosphate fertilizers. **ACS Sustainable Chemistry and Engineering.** v. 11, p. 14203–14212, 2018.

CHEN, S.; WANG, J.; WU, Z.; DENG, Q.; TU, W.; DAI, Z.; ZHENG, S.; DENG. Enhanced Cr(VI) removal by polyethylenimine- and phosphorus-codoped hierarchical porous carbons. **Journal of Colloid and Interface Science**, v. 523, p. 110-120, 2018.

CHEN, H.; LI, W.; WANG, J.; XU, H.; LUI, Y.; ZHANG, Z.; LI, Y.; ZHANG, Y. Adsorption of cadmium and lead ions by phosphoric acid-modified biochar generated from chicken feather: Selective adsorption and influence of dissolved organic matter. **Bioresource Technology**, v. 292, p. 121948, 2019a.

CHEN, H.; ZHANG, J.; TANG, L.; SU, M.; TIAN, D.; ZHANG, L.; LI, Z.; HU, S. Enhanced Pb immobilization via the combination of biochar and phosphate solubilizing bacteria. **Environment International**, v. 127, p. 395-401, 2019b.

CHOWDHURY, I. H.; CHOWDHURY, A. H.; BOSE, P.; MANDAL, S.; NASKAR, M. K. Effect of anion type on the synthesis of mesoporous nanostructured MgO, and its excellent adsorption capacity for the removal of toxic heavy metal ions from water. **RSC Advanced**, v. 6, p. 6038–6047, 2016.

CAO, X.; MA, L.; GAO, B.; HARRIS, W. Dairy-manure derived biochar effectively sorbs lead and atrazine. **Environmental Science and Technology**, v. 43, p. 3285–3291, 2009.

CUI, L.; CHEN, T.; YIN, C.; YAN, J.; IPPOLITO, J.A.; HUSSAIN, Q. Mechanism of adsorption of cadmium and lead ions by iron-activated biochar. **Bioresources**, v. 14, p. 842 – 857, 2019.

DALÓLIO, F. S.; SILVA, J. N.; OLIVEIRA, A. C. C.; TINOCO, I. F. F.; BARBOSA, R. C.; RESENDE, M. O.; ALBINO, F. L. T., COELHO, S. T. Poultry litter as biomass energy: A review and future perspectives. **Renewable and Sustainable Energy Reviews**, v. 76, p. 941-949, 2017.

DEWAGE, B. D.; FOWLER, R. E.; PITTMAN Jr., C.U.; MOHAN, D.; MLSNA, T. Lead (Pb^{2+}) sorptive removal using chitosan-modified biochar: batch and fixed-bed studies. **RSC Advanced**, v. 8, p. 25368-25377, 2018.

FAHMI, A. H.; SAMSURI, A.W.; JOL, H.; SINGH, D. Physical modification of biochar to expose the inner pores and their functional groups to enhance lead adsorption. **RSC Advanced,** v. 8, p. 38270-38280, 2018.

GAO, R.; FU, Q.; HU, H.; LIU, Y.; ZHU, J. Highly-effective removal of Pb by co-pyrolysis biochar derived from rape straw and orthophosphate. **Journal of Hazardous Materials**, v. 371, p. 191-197, 2019.

JIN, Z.; JIA, Y.; ZHANG, K.S.; KONG, L.T.; SUN, B.; SHEN, W.; LIU, J.H. Effective removal of fluoride by porous MgO nanoplates and its adsorption mechanism. **Journal of Alloys and Compounds**, v. 675, p. 292–300, 2016.

KABATA-PENDIAS, A. **Trace Elements in Soils and Plants**. 4. ed., CRC Press, 2011.

KARUNANAYAKE, A. G.; TODD, O. A.; CROWLEY, M.; RICCHETTI, L.; PITTMAN JR., C.U.; ANDERSON, R.; MOHAN, D.; MLSNA, T. Lead and cadmium remediation using magnetized and nonmagnetized biochar from Douglas fir. **Chemical Engineering Journal**, v. 331, p. 480-491, 2018.

LEE, M.; PARK, J. H.; CHUNG, J. W. Comparison of the lead and copper adsorption capacities of plant source materials and their biochars. **Journal of Environmental Management**, v. 236, p. 118-124, 2019.

LEI, S.; SHI., QIU, Y.; CHEN, L.; XUE, C. Performance and mechanisms of emerging animal-derived biochars for immobilization of heavy metals. **Science of the Total Environment**, v. 646, p.1281–1289, 2019.

LI, R.; LIANG, W.; WANG, J. J; GASTON, L. A.; HUANG, D.; HUANG, H.; LEI, S.; AWASTHI, M. K.; ZHOU, B.; XIAO, R.; ZHANG, Z. Facilitative capture of As(V), Pb(II) and methylene blue from aqueous solutions with MgO hybrid sponge-like carbonaceous composite derived from sugarcane leafy trash. **Journal of Environmental Management**, v. 212, p. 77–87, 2018.

LI, J.; ZHENG, L.; WANG, S.; WU, Z.; WU, W.; NIAZI, N. K.; SHAHEEN, S. M.; RINKLEBE, J.; BOLAN, N.; OK, Y.S.; WANG, H. Sorption mechanisms of lead on silicon-rich biochar in aqueous solution: Spectroscopic investigation. **Science of the Total Environment**, v. 672, p. 572-582, 2019.

LING, L.; LIU, W.; ZHANG, S.; JIANG, H. Magnesium Oxide Embedded Nitrogen Self-doped Biochar Composites: Fast and High-efficiency Adsorption of Heavy Metals in an Aqueous Solution. **Environmental Science and Technology**, v. 51, p. 10081-10089, 2017.

LUSTOSA FILHO, J. F.; PENIDO, E. S.; CASTRO, P. P.; SILVA, C. A.; MELO, L. C. A. Co-Pyrolysis of Poultry Litter and Phosphate and Magnesium Generates Alternative Slow-Release Fertilizer Suitable for Tropical Soils. **ACS Sustainable Chemistry and Engineering**, v. 10, p. 9043–9052, 2017.

LUSTOSA FILHO, J.F.; BARBOSA, C. F.; CARNEIRO, J. S. S.; MELO, L. C. A. Diffusion and phosphorus solubility of biochar-based fertilizer: Visualization, chemical assessment and availability to plants. **Soil and Tillage Research**, v. 194, p. 104298, 2019.

MIRELES, S.; PARSONS, J.; TRAD, T.; CHENG, C. L.; KANG, J. Lead removal from aqueous solutions using biochars derived from corn stover, orange peel, and pistachio shell. **International Journal of Environmental Science and Technology**, p. 1-10, 2019.

PATRICK., L. Lead toxicity, a review of the literature. Part 1: exposure, evaluation, and treatment. **Alter. Med. Rev.,** v. 11, p. 2, 2006.

PENIDO, E. S.; MELO, L. C. A.; GUILHERME, L. R. G.; BIANCHI, M. L. Cadmium binding mechanisms and adsorption capacity by novel phosphorus/magnesium-engineered biochars. **Science of the Total Environment**, v. 671, p. 1134-1143, 2019.

PENG, H., GAO, P., CHU, G., PAN, B., PENG, J., XING, B. Enhanced adsorption of Cu(II) and Cd(II) by phosphoric acid-modified biochars. **Environmental Pollution**, v. 229, p. 846-853, 2017.

PREMARATHNA, K. S. D.; RAJAPAKSHA, A. U.; SARKAR, B.; KWON, E. E.; BHATNAGAR, A.; OK, Y.S.; VITHANAGE, M. Biochar-based engineered composites for sorptive decontamination of water: A review. **Chemical Engineering Journal**, v. 372, p. 536–550, 2019.

QAMBRANI, N. A.; RAHMAN, M. M.; WON, S.; SHIM, S.; RA, C. Biochar properties and eco-friendly applications for climate change mitigation, waste management, and wastewater treatment: a review. **Renewable Sustainable Energy Reviews**, v. 79, p. 255-273, 2017.

SANDERSON, P.; NAIDU, R.; BOLAN, N.; LIM, J. E.; OK, Y. S. Chemical stabilisation of lead in shooting range soils with phosphate and magnesium oxide: Synchrotron investigation. **Journal of Hazardous Materials**, v. 299, p. 395–403, 2015.

SHEN, Z.; HOU, D.; JIN, F.; SHI, J.; FAN, X.; TSANG, D. C. J.; ALESSI, D. S. Effect of production temperature on lead removal mechanisms by rice straw biochars. **Science of the Total Environment**, v. 655, p. 751-758, 2019.

SILVERSTEIN, R. M.; WEBSTER, F. X.; KIEMLE, D. J.; BRYCE, D. L. **Spectrometric Identification of Organic Compounds**, 8. Ed. Wiley, 2014, 464 Pages.

SIZMUR, T.; FRESNO, T.; AKGÜL, G.; FROST, H.; JIMÉNEZ, E. M. Biochar modification to enhance sorption of inorganics from water. **Bioresource Technology**, v. 246, p. 34-47, 2017.

UCUN, H.; BAYHANA, Y. K.; KAYA, Y.; CAKICI, A.; ALGUR, O. F. Biosorption of lead (II) from aqueous solution by cone biomass of Pinus sylvestris. **Desalination**, v. 154, p. 233–238, 2003.

UNITED STATES ENVIRONMENTAL PROTECTION AGENCY - USEPA, Toxicity characteristic leaching procedure, method 1311, 1992. Disponível em https://www.epa.gov/sites/production/files/2015-12/documents/1311.pdf.

WANG, H.; GAO, B.; FANG, J.; OK, Y. S.; XUE, Y.; YANG, K.; CAO, X. Engineered biochar derived from eggshell-treated biomass for removal of aqueous lead. **Ecological Engineering**, v. 121, v. 1, p 124-129, 2018.

WANG, J.; WANG, S. Preparation, modification and environmental application of biochar: A review. **Journal of Cleaner Production**, v. 227, p. 1002-1022, 2019.

WEI, S., ZHU, M., FAN, X., SONG, J., PENG, P., LI, K., JIA, W., SONG, H. Influence of pyrolysis temperature and feedstock on carbon fractions of biochar produced from pyrolysis of rice straw, pine wood, pig manure and sewage sludge. **Chemosphere**, v. 218, p. 624-631, 2019.

WU, W.; LI, J.; LAN, T.; MÜLLER, K.; NIAZI, N. K.; CHEN, X.; XU, S.; ZHENG, L.; CHU, Y.; LI, J.; YUAN, G.; WANG, H. Unraveling sorption of lead in aqueous solutions by chemically modified biochar derived from coconut fiber: a microscopic and spectroscopic investigation. **Science of the Total Environment**, v. 576, p. 766-774, 2017.

XIONG, J.; KOOPAL, L. K; TAN, W.F.; FANG, L.C.; WANG, M.X.; ZHAO, W.; LIU, F.; ZHANG, J.; WENG, L.P. Lead binding to soil fulvic and humic acids: NICA-Donnan modeling and XAFS spectroscopy. **Environmental Science and Technology**, 2013.

XU, X.; HU, X.; DING, Z.; CHEN, Y. Effects of copyrolysis of sludge with calcium carbonate and calcium hydrogen phosphate on chemical stability of carbon and release of toxic elements in the resultant biochars. **Chemosphere**, v. 189, p. 6−85, 2017.

YANG, F.; ZHANG, S.; CHO, D.; DU, Q.; SONG, J.; TSANG, D. C. W. Porous biochar composite assembled with ternary needle-like iron-manganese-sulphur hybrids for high-efficiency lead removal. **Bioresource Technology**, v. 272, p. 415-420, 2019.

ZHAO, L.; CAO, X.; ZHENG, W.; SCOTT, J. W.; SHARMA, B. K.; CHEN, X., 2016. Copyrolysis of biomass with phosphate fertilizers to improve biochar carbon retention, slow nutrient release, and stabilize heavy metals in soil. **ACS Sustainable Chemistry and Engineering**, v. 4, p. 1630−1636, 2016.

ZHANG, Y.; CAO, B.; ZHAO, L.; SUN, L.; GAO, Y.; LI, J. J.; YANG, F. Biochar-supported reduced graphene oxide composite for adsorption and coadsorption of atrazine and lead ions. **Applied Surface Science**, v. 427, p. 147-155, 2018.

ZHANG, J.; SHAO, J.; JIN, Q.; LI, Z.; ZHANG, X.; CHEN, Y.; ZHANG, S.; CHEN, H. Sludge-based biochar activation to enhance Pb(II) adsorption. **Fuel**, v. 252, p. 101-108, 2019.

ZHOU, Z., XU, Z., FENG, Q., YAO, D., YU, J., WANG, D., LV, S., LIU, Y., ZHOU, N., ZHONG, M. Effect of pyrolysis condition on the adsorption mechanism of lead, cadmium and copper on tobacco stem biochar. **Journal of Cleaner Production**, v. 187, p. 996-1005, 2018.

APPENDIX A

Supplementary material

The pseudo first-order (Equation 1) and pseudo second-order (Equation 2) models (linear equations) were used for assessing the reaction order of Pb^{2+} adsorption onto biochars in the kinetic experiment.

$$\ln(q_e - q_t) = \ln q_e - k_1 t \quad (1)$$

$$\frac{t}{q_t} = \frac{1}{k_2 q_e^2} + \frac{t}{q_e} \quad (2)$$

in which q_t is the amount of Pb^{2+} adsorbed (mg g^{-1}) at time t, q_e is the amount of Pb^{2+} adsorbed (mg g^{-1}) at equilibrium time, and k_1 (h^{-1}) and k_2 (g mg^{-1} h^{-1}) are the rate constants of the pseudo first-order equation and pseudo second-order equation, respectively.

Figure A. Pseudo-first-order and pseudo-second-order kinetic models for the studied biochars.

pseudo first-order

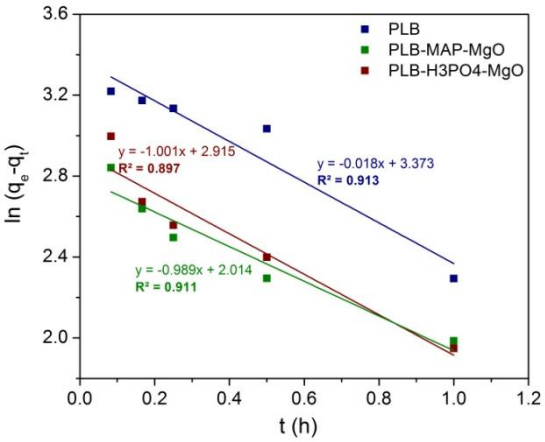

pseudo second-order

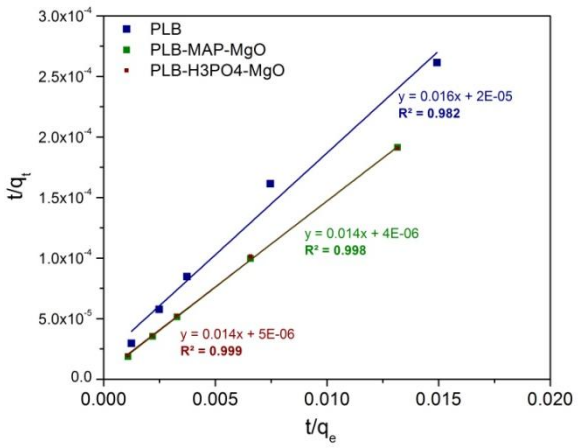

The amount of Pb^{2+} adsorbed per unit mass of adsorbent was calculated from the following expression:

$$q_{eq} = \frac{(C_0 - C_{eq}) \times V}{m} \quad (1)$$

where q_e (mg g^{-1}) was the amount of Pb^{2+} adsorbed; C_0 and C_{eq} (mg L^{-1}) were the initial and equilibrium Pb^{2+} concentrations in the aqueous solution; V (L) was the volume of the solution and m (g) was the adsorbent dose.

Figure B. Photographs of biochars after Pb^{2+} adsorption in aqueous medium, showing a white precipitate for P/Mg-engineered biochars. No white precipitate was visually observed for PLB.

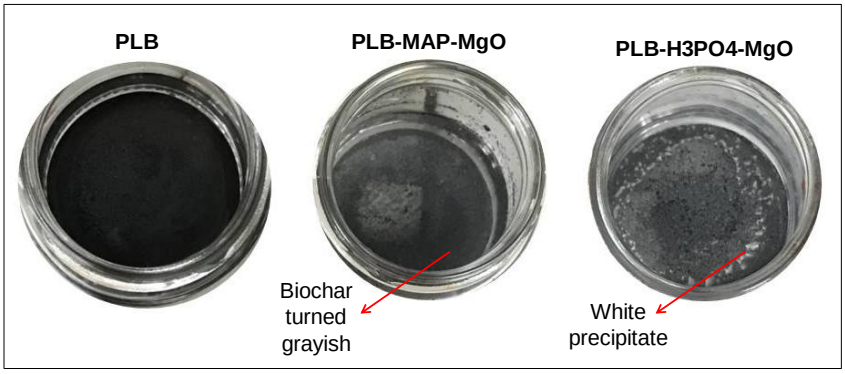

Source: from author (2019).

REFERENCES

LING, L.; LIU, W.; ZHANG, S.; JIANG, H. Magnesium Oxide Embedded Nitrogen Self-doped Biochar Composites: Fast and High-efficiency Adsorption of Heavy Metals in an Aqueous Solution. **Environmental Science and Technology**, v. 17, p. 10081-10089, 2017.

MOHAN, D.; KUMAR, H.; SARSWAT, A.; ALEXANDRE-FRANCO, M.; PITTMAN, C.U. Cadmium and lead remediation using magnetic oak wood and oak bark fast pyrolysis bio-chars. **Chemical Engineering Journal**, v. 236, p. 513-528, 2014

WANG, S.; GAO, B.; LI, Y.; MOSA, A.; ZIMMERMAN, A. R.; MA, L. Q.; HARRIS, W. G.; MIGLIACCIO, K. W. Manganese oxide-modified biochars: preparation, characterization, and sorption of arsenate and lead. **Bioresource Technology**, v. 181, p. 13 - 17, 2015.

WANG, Z.; LIU, G.; ZHENG, H.; LI, F.; NGO, H. H.; GUO, W.; LIU, C.; CHEN, L.; XING, B. Investigating the mechanisms of biochar's removal of lead from solution. **Bioresource Technology**, v. 177, p. 308-317, 2015.

WU, W.; LI, J.; NIAZI, N.K.; MÜLLER, K.; CHU, Y.; ZHANG., L.; YUAN, G.; LU, K.; SONG, Z.; WANG, H. Influence of pyrolysis temperature on lead immobilization by chemically modified coconut fiber-derived biochars in aqueous environments. **Environmental Science and Pollution Research**, v. 23, p. 22890–22896, 2016.

XU, T.; LIU, X. Q. Peanut shell activated carbon: Characterization, surface modification and adsorption of Pb^{2+} from aqueous solution. **Chinese Journal of Chemical Engineering**, v. 16, p. 401–406, 2008.

XUE, Y. W.; GAO, B.; YAO, Y.; INYANG, M.; ZHANG, M.; ZIMMERMAN, A. R.; ANDRO, K. S. Hydrogen peroxide modification enhances the ability of biochar (hydrochar) produced fromhydrothermal carbonization of peanut hull to remove aqueous heavy metals: Batch and column tests. **Chemical Engineering Journal**, v. 200, p. 673 – 680, 2012.